Interaction of excited states in two-species Bose-Einstein condensates: a case study

Todd Kapitula *
Department of Mathematics and Statistics
Calvin College
Grand Rapids, MI 49546

Kody J.H. Law †
Department of Mathematics and Statistics
University of Massachusetts
Amherst, MA 01003-4515

Panayotis G. Kevrekidis ‡
Department of Mathematics and Statistics
University of Massachusetts
Amherst, MA 01003-4515

July 9, 2009

Abstract. In this paper we consider the existence and spectral stability of excited states in two-species Bose-Einstein condensates in the case of a pancake magnetic trap. Each new excited state found in this paper is to leading order a linear combination two one-species dipoles, each of which is a spectrally stable excited state for one-species condensates. The analysis is done via a Lyapunov-Schmidt reduction and is valid in limit of weak nonlinear interactions. Some conclusions, however, can be made at this limit which remain true even when the interactions are large.

*E-mail: tmk5@calvin.edu
†E-mail: law@math.umass.edu
‡E-mail: kevrekid@math.umass.edu

Contents

1. Introduction 1

2. Existence 3
   2.1. Lyapunov-Schmidt reduction 3
   2.2. Real-valued solutions 4
   2.3. Complex-valued solutions 5

3. Stability: small eigenvalues 7
   3.1. Reduced eigenvalue problem: theory 8
   3.2. Reduced eigenvalue problem: real-valued solutions 10
      3.2.1. In-phase dipole-dipole 10
      3.2.2. Out-of-phase dipole-dipole 10
   3.3. Reduced eigenvalue problem: complex-valued solutions 11
      3.3.1. Vortex-vortex 11
      3.3.2. Azimuthon-dipole 12
      3.3.3. Dipole-azimuthon 12

4. Stability: Hamiltonian-Hopf bifurcations 13
   4.1. Reduced eigenvalue problem: theory 13
   4.2. Reduced eigenvalue problem: real-valued solutions 14
      4.2.1. In-phase dipole-dipole 14
      4.2.2. Out-of-phase dipole-dipole 16
   4.3. Reduced eigenvalue problem: complex-valued solutions 17
      4.3.1. Vortex-vortex 17

5. Numerical results 18
   5.1. Numerical existence and stability 18
   5.2. Dynamics of spectrally unstable states 19

References 20

1. Introduction

Over the past decade the experimental realization of Bose-Einstein condensates (BECs) has triggered a continuously expanding interest in the study of fundamental quantum phenomena as well as of nonlinear waves that arise in this setting [29, 41, 42]. From a theoretical and modeling perspective the presence of a mean-field model that has been established as accurately describing the condensate dynamics near zero temperature has led to a wide range of studies on the solitary waves and coherent structures that emerge in the BECs. The macroscopic nonlinear matter waves that arise due to the nonlinear inter-particle interaction which have been explored both theoretically and experimentally include: bright solitons in quasi-one-dimensional attractive BECs [30, 47], dark [3, 9, 12, 13] and gap [14] matter-wave solitons in quasi-one-dimensional repulsive BECs, and vortices [33, 34] and vortex lattices [2, 15] in higher dimensions.

Multi-component BECs may arise either between coupled hyperfine states of a single species, or between two different atomic species, and a principal aspect of interest in this setting has been the statics and dynamics of binary mixtures [20, 37, 45]. A particularly important manifestation of the interspecies interactions has been the display of rich phase separation dynamics. The latter leads, e.g., to the formation of robust single- and multi-ring patterns [20, 35], the evolution of initially coincident triangular vortex lattice through a turbulent regime into an interlaced square vortex lattice [44] in coupled hyperfine states of ^{87}Rb, or the study in optical traps of different Zeeman levels of ^{23}Na forming striated magnetic domains [36, 46]. Experimental efforts are still very active in a number of directions and include a detailed examination of the observed phase separation phenomenology [**35**], as well as the study of structural phase transitions from the immiscible to the miscible regime [**38**].

In parallel to, or often preceding, these experimental studies, a large volume of theoretical work has been done which has significantly contributed to a more detailed understanding of such multi-component BECs. Among the topics considered, one may highlight the stability of BECs against excitations [**5**, **17**, **21**, **31**], their static and dynamics properties [**10**, **16**, **18**, **19**, **43**], and the study of solitary waves [**7**, **28**, **40**, **49**].

Our aim in the present work is to analytically consider the interaction of excited states in a two-component system. The analysis is tractable because it is based upon the well-understood linear limit, i.e., the weak nonlinear interaction limit. We will not do an exhaustive study of all possible interactions; instead, we will focus upon a particular case which nicely illustrates the possibilities associated with intra-species interactions. For a one-component system the dipole is a real-valued excited state which is spectrally stable (at least in the limit of weak interactions). The associated complex-valued excited state, which is again spectrally stable, is the radially symmetric vortex of charge one. In this paper we are interested in seeing if the nonlinear intra-species interactions lead to new excited states which are not simply a dipole/dipole, dipole/vortex, or vortex/vortex combination. The answer will be a function of the system parameters: the relative strengths of the intra-species and inter-species nonlinearities (i.e., the specific values of a_1 and a_2 given in Eq. (1.2)), and the relative number of atoms in each of the components. In addition to the expected solutions there will be a new type of solution, namely the azimuthon-dipole. This solution has the property that it is a dipole in one component and a non-radially symmetric vortex of charge one in the other component. Even though the one-component solutions are spectrally stable, many of the two-component solutions will be spectrally unstable in some parameter regimes. The reader should consult Figure 1 for a graphical depiction of the stability bifurcation diagram.

The governing equations for a two-species Bose-Einstein condensate are given by

$$\mathrm{i}\partial_t q_j + \Delta q_j + \omega_j q_j + \sum_{k=1}^{2} a_{jk}|q_k|^2 q_j = V(\boldsymbol{x})q_j, \quad j = 1, 2, \tag{1.1}$$

where the complex-valued q_j is the mean-field wave-function of species j, $a_{jk} \in \mathbb{R}$ with $a_{12} = a_{21}$, $\omega_j \in \mathbb{R}$ is a free parameter and represents the chemical potential for each species, and $V(\boldsymbol{x}) : \mathbb{R}^2 \mapsto \mathbb{R}$ represents the trapping potential (see [**1**, **4**, **6**, **8**, **10**, **27**, **28**, **34**] and the references therein for further details). In this paper it will be assumed that both the intra-species and inter-species interactions are repulsive, i.e., $a_{jk} \in \mathbb{R}^-$. A simple rescaling via $q_j \mapsto |a_{21}|^{1/2} q_j$ maps $a_{21} \mapsto \mathrm{sign}(a_{21})$ and $a_{jj} \mapsto a_{jj}/|a_{21}|$. Set $a_j := -a_{jj}/|a_{12}| \in \mathbb{R}^+$. Assume now that only a magnetically induced parabolic trapping potential is present, which implies that $V(\boldsymbol{x}) = |\boldsymbol{x}|^2$. One can now rewrite Eq. (1.1) as

$$\begin{aligned} &\mathrm{i}\partial_t q_1 + \Delta q_1 + \omega_1 q_1 - \left(a_1|q_1|^2 + |q_2|^2\right) q_1 = |\boldsymbol{x}|^2 q_1 \\ &\mathrm{i}\partial_t q_2 + \Delta q_2 + \omega_2 q_2 - \left(|q_1|^2 + a_2|q_2|^2\right) q_2 = |\boldsymbol{x}|^2 q_2. \end{aligned} \tag{1.2}$$

Finally, for $\epsilon > 0$ scale the wave-functions by $q_j \mapsto \epsilon^{1/2}\tilde{q}_j$, and note that $\epsilon \ll 1$ implies that $\iint |q_j|^2 \,\mathrm{d}\boldsymbol{x} = \mathcal{O}(\epsilon)$. Upon dropping the tilde Eq. (1.2) becomes

$$\begin{aligned} &\mathrm{i}\partial_t q_1 + \Delta q_1 + \omega_1 q_1 - \epsilon\left(a_1|q_1|^2 + |q_2|^2\right) q_1 = |\boldsymbol{x}|^2 q_1 \\ &\mathrm{i}\partial_t q_2 + \Delta q_2 + \omega_2 q_2 - \epsilon\left(|q_1|^2 + a_2|q_2|^2\right) q_2 = |\boldsymbol{x}|^2 q_2. \end{aligned} \tag{1.3}$$

This is the system to be studied in this paper.

The paper is organized as follows. In Section 2 we find steady-state solutions to Eq. (1.3) for $0 < \epsilon \ll 1$. This task will be accomplished via a Lyapunov-Schmidt reduction. In Section 3 and Section 4 the spectral stability of these solutions is determined. In addition to completely determining the location of the $\mathcal{O}(\epsilon)$ eigenvalues (Section 3), we will partially determine the location of the eigenvalues associated with a potential Hamiltonian-Hopf bifurcation (Section 4). Finally, in Section 5 we numerically verify some of the analytical results for the parameter regime of physical interest, as well as give an indication of the dynamics associated with the evolution of spectrally unstable solutions.

Acknowledgments. TK gratefully acknowledges the support of the Jack and Lois Kuipers Applied Mathematics Endowment, a Calvin Research Fellowship, and the National Science Foundation under grant

DMS-0806636. PGK gratefully acknowledges support from NSF-CAREER (NSF-DMS-0349023), NSF-DMS-0505663 and NSF-DMS-0806762, as well as from the Alexander von Humboldt Foundation.

2. Existence

2.1. Lyapunov-Schmidt reduction

In order to perform the Lyapunov-Schmidt reduction, it is important that one has a thorough understanding of $\sigma(\mathcal{L})$, where for $r := |\boldsymbol{x}|$,

$$\begin{aligned}\mathcal{L} &:= -\Delta + r^2 \\ &= -\partial_r^2 - \frac{1}{r}\partial_r - \frac{1}{r^2}\partial_\theta^2 + r^2.\end{aligned} \tag{2.1}$$

If one uses a Fourier decomposition and writes

$$q(r,\theta) = \sum_{\ell=-\infty}^{+\infty} q_\ell(r)\mathrm{e}^{\mathrm{i}\ell\theta}, \tag{2.2}$$

then the eigenvalue problem $\mathcal{L}q = \lambda q$ becomes the infinite sequence of linear Schrödinger eigenvalue problems in the radial variable for $\ell \in \mathbb{Z}$:

$$\mathcal{L}_\ell q_\ell = \lambda q_\ell, \quad \mathcal{L}_\ell := -\partial_r^2 - \frac{1}{r}\partial_r + \frac{\ell^2}{r^2} + r^2. \tag{2.3}$$

Concerning the operator $\mathcal{L}_\ell$ it is well-known that for each fixed $\ell \in \mathbb{Z}$ there is a countably infinite sequence of simple eigenvalues $\{\lambda_{m,\ell}\}_{m=0}^{\infty}$, with

$$\lambda_{m,\ell} := 2(|\ell| + 1) + 4m, \tag{2.4}$$

such that the eigenfunction $q_{m,\ell}(r)$ corresponding to $\lambda_{m,\ell}$ has precisely m zeros. With respect to the operator $\mathcal{L}$ one then has that for each $\lambda_{m,\ell}$ there exist the real-valued eigenfunctions $q_{m,\ell}(r)\cos(\ell\theta)$ and $q_{m,\ell}(r)\sin(\ell\theta)$. This implies that if $\ell \neq 0$, then the eigenvalue is not simple, and has geometric multiplicity no smaller than two. Finally, it is known that if $\lambda \in \sigma(\mathcal{L})$, then $\lambda = \lambda_{m,\ell}$ for some pair $(m,\ell) \in \mathbb{N}_0 \times \mathbb{Z}$. Since $\lambda_{m,\ell} = \lambda_{m',\ell'}$ if and only if

$$\ell' - \ell = 2(m - m'), \tag{2.5}$$

the operator $\mathcal{L}$ has semisimple eigenvalues with multiplicity greater than two for $m + |\ell| \geq 2$. The eigenfunctions associated with these eigenvalues are linear excited states.

The set-up is now complete in order to compute the series expansion which will be used to analytically study the intra-species interactions of excited states. The first excited state occurs when $(m,\ell) = (0,1)$, i.e., $\lambda = 4$; furthermore, for this case one has that

$$\ker(\mathcal{L} - \lambda_{0,1}) = \mathrm{Span}\{q_{0,1}(r)\cos\theta, q_{0,1}(r)\sin\theta\}; \quad q_{0,1}(r) = \sqrt{\frac{2}{\pi}}\, r\mathrm{e}^{-r^2/2}. \tag{2.6}$$

Upon referring to Eq. (2.6) set

$$\boldsymbol{q}_1 := q_{0,1}(r)\cos\theta, \quad \boldsymbol{q}_2 := q_{0,1}(r)\sin\theta. \tag{2.7}$$

Performing a Taylor expansion for the chemical potentials, one will have for $j = 1, 2$,

$$\omega_j = \lambda_{0,1} + \Delta\omega_j\,\epsilon + \mathcal{O}(\epsilon^2).$$

Upon setting

$$\Delta\omega := \Delta\omega_1, \quad b := \frac{\Delta\omega_2}{\Delta\omega_1},$$

for the steady-state problem associated with Eq. (1.3) write

$$\begin{aligned} q_1 &= x_1\boldsymbol{q}_1 + x_2\boldsymbol{q}_2 + \mathcal{O}(\epsilon), \quad \omega_1 = \lambda_{0,1} + \Delta\omega\,\epsilon + \mathcal{O}(\epsilon^2) \\ q_2 &= y_1\boldsymbol{q}_1 + y_2\boldsymbol{q}_2 + \mathcal{O}(\epsilon), \quad \omega_2 = \lambda_{0,1} + b\Delta\omega\,\epsilon + \mathcal{O}(\epsilon^2), \end{aligned} \tag{2.8}$$

where $x_j, y_j \in \mathbb{C}$ for $j = 1, 2$. Now, Eq. (1.3) is invariant under the gauge symmetry $q_j \mapsto q_j \mathrm{e}^{\mathrm{i}\phi_j}$, and under the spatial SO(2) symmetry of rotation. The equivariant Lyapunov-Schmidt bifurcation theory guarantees that the bifurcation equations have the same symmetries as the underlying system (e.g., see [**11**]). Consequently, without loss of generality one may assume in Eq. (2.8) that $x_1, y_1 \in \mathbb{C}$ and $x_2, y_2 \in \mathrm{i}\mathbb{R}$. The expansion of Eq. (2.8) then becomes

$$\begin{aligned} q_1 &= x_1\boldsymbol{q}_1 + \mathrm{i}x_2\boldsymbol{q}_2 + \mathcal{O}(\epsilon), \quad \omega_1 = \lambda_{0,1} + \Delta\omega\,\epsilon + \mathcal{O}(\epsilon^2) \\ q_2 &= y_1\boldsymbol{q}_1 + \mathrm{i}y_2\boldsymbol{q}_2 + \mathcal{O}(\epsilon), \quad \omega_2 = \lambda_{0,1} + b\Delta\omega\,\epsilon + \mathcal{O}(\epsilon^2), \end{aligned} \tag{2.9}$$

where now one has that $x_1, y_1 \in \mathbb{C}$, and $x_2, y_2 \in \mathbb{R}$. Substitution of the expansion of Eq. (2.9) into the steady-state associated with Eq. (1.3) and an application of the Lyapunov-Schmidt reduction yields the following set of bifurcation equations:

$$\begin{aligned} 0 &= -\mu x_1 + a_1(3|x_1|^2 x_1 + 2x_1 x_2^2 - \overline{x_1} x_2^2) + (3|y_1|^2 + y_2^2)x_1 + (y_1 - \overline{y_1})x_2 y_2 \\ 0 &= -\mu x_2 + a_1(3x_2^3 + 2|x_1|^2 x_2 - x_1^2 x_2) + (|y_1|^2 + 3y_2^2)x_2 - (y_1 - \overline{y_1})x_1 y_2 \\ 0 &= -b\mu y_1 + a_2(3|y_1|^2 y_1 + 2y_1 y_2^2 - \overline{y_1} y_2^2) + (3|x_1|^2 + x_2^2)y_1 + (x_1 - \overline{x_1})x_2 y_2 \\ 0 &= -b\mu y_2 + a_2(3y_2^3 + 2|y_1|^2 y_2 - y_1^2 y_2) + (|x_1|^2 + 3x_2^2)y_2 - (x_1 - \overline{x_1})x_2 y_1, \end{aligned} \tag{2.10}$$

where

$$\mu := \frac{\Delta\omega}{g}, \quad g := \frac{\pi}{4}\int_0^\infty r q_{0,1}^4(r)\,\mathrm{d}r \ \left(= \frac{1}{8\pi}\right). \tag{2.11}$$

Note that $\mathrm{sign}(\mu) = \mathrm{sign}(\Delta\omega)$. The remainder of this section will be devoted to the analysis of Eq. (2.10).

2.2. *Real-valued solutions*

Let us first consider the case of real-valued solutions. One sees from Eq. (2.9) that one set can be found by setting $(x_2, y_2) = (0, 0)$ with $x_1, y_1 \in \mathbb{R}$. In this case Eq. (2.10) reduces to

$$\begin{aligned} 0 &= x_1\left[-\mu + 3a_1 x_1^2 + 3y_1^2\right] \\ 0 &= y_1\left[-b\mu + 3x_1^2 + 3a_2 y_1^2\right]. \end{aligned} \tag{2.12}$$

The solution to Eq. (2.12) which is nonzero in both components is given by

$$\begin{pmatrix} x_1^2 \\ y_1^2 \end{pmatrix} = \frac{\mu}{3(a_1 a_2 - 1)}\begin{pmatrix} a_2 - b \\ b a_1 - 1 \end{pmatrix}. \tag{2.13}$$

Note that the solution given in Eq. (2.13) is valid if and only if $(ba_1 - 1)(a_2 - b) > 0$, i.e.,

$$\begin{aligned} a_1 a_2 > 1 &: 1/a_1 \le b \le a_2 \\ a_1 a_2 < 1 &: a_2 \le b \le 1/a_1. \end{aligned} \tag{2.14}$$

Note that in either case $\mu > 0$. Further note that if one considers, e.g., the case of $a_1 a_2 > 1$, then $b = 1/a_1$ corresponds to the solution with $q_2 \equiv 0$, and $b = a_2$ corresponds to the solution with $q_1 \equiv 0$. From Eq. (2.7) and Eq. (2.9) it is seen that this solution corresponds to in-phase dipoles.

Another real-valued solution to Eq. (2.10) can be found by setting $(x_2, y_1) = (0, 0)$ and assuming that $x_1 \in \mathbb{R}$. Eq. (2.10) then reduces to

$$\begin{aligned} 0 &= x_1\left[-\mu + 3a_1 x_1^2 + y_2^2\right] \\ 0 &= y_2\left[-b\mu + x_1^2 + 3a_2 y_2^2\right], \end{aligned} \tag{2.15}$$

and the solution to Eq. (2.15) which is nonzero in both components is

$$\begin{pmatrix} x_1^2 \\ y_2^2 \end{pmatrix} = \frac{\mu}{9a_1a_2 - 1} \begin{pmatrix} 3a_2 - b \\ 3ba_1 - 1 \end{pmatrix}. \tag{2.16}$$

Note that the solution given in Eq. (2.16) is valid if and only if $(3ba_1 - 1)(3a_2 - b) > 0$, i.e.,

$$\begin{aligned} a_1a_2 > 1/9 &: 1/3a_1 \le b \le 3a_2 \\ a_1a_2 < 1/9 &: 3a_2 \le b \le 1/3a_1. \end{aligned} \tag{2.17}$$

From Eq. (2.7) and Eq. (2.9) it is seen that this solution corresponds to out-of-phase dipoles.

It is not difficult to show that any other solution to Eq. (2.10) which represents a real-valued solution is equivalent via the symmetries to that presented in either Eq. (2.13) or Eq. (2.16). In summary, the following result has now been proven.

Lemma 2.1. *The in-phase dipole-dipole solution to Eq. (1.3) is given by*

$$q_1 \sim \sqrt{\frac{a_2 - b}{3(a_1a_2 - 1)g}\Delta\omega}\, q_{0,1}(r)\cos\theta \qquad q_2 \sim \sqrt{\frac{ba_1 - 1}{3(a_1a_2 - 1)g} b\Delta\omega}\, q_{0,1}(r)\cos\theta,$$

where $\Delta\omega > 0$. The restrictions on b are given in Eq. (2.14). The out-of-phase dipole-dipole solution to Eq. (1.3) is given by

$$q_1 \sim \sqrt{\frac{3a_2 - b}{(9a_1a_2 - 1)g}\Delta\omega}\, q_{0,1}(r)\cos\theta, \qquad q_2 \sim \sqrt{\frac{3ba_1 - 1}{(9a_1a_2 - 1)g} b\Delta\omega}\, q_{0,1}(r)\sin\theta,$$

where $\Delta\omega > 0$. The restrictions on b are given in Eq. (2.17).

2.3. *Complex-valued solutions*

Now consider complex-valued solutions to Eq. (2.10). Upon setting

$$x_1 := \rho_1 e^{i\phi_1}, \quad y_1 := s_1 e^{i\psi_1}, \tag{2.18}$$

the imaginary part of Eq. (2.10) can be written as

$$\begin{aligned} \begin{pmatrix} 0 \\ 0 \end{pmatrix} &= \begin{pmatrix} \rho_1\cos\phi_1 & 0 \\ 0 & s_1\cos\psi_1 \end{pmatrix} \begin{pmatrix} a_1 & 1 \\ 1 & a_2 \end{pmatrix} \begin{pmatrix} \rho_1 x_2 \sin\phi_1 \\ s_1 y_2 \sin\psi_1 \end{pmatrix} \\ \begin{pmatrix} 0 \\ 0 \end{pmatrix} &= \begin{pmatrix} -\mu + 3a_1(\rho_1^2 + x_2^2) + 3s_1^2 + y_2^2 & 2x_2y_2 \\ 2x_2y_2 & -b\mu + 3\rho_1^2 + x_2^2 + 3a_2(s_1^2 + y_2^2) \end{pmatrix} \begin{pmatrix} \rho_1\sin\phi_1 \\ s_1\sin\psi_1 \end{pmatrix}, \end{aligned} \tag{2.19}$$

and the real part of Eq. (2.10) becomes

$$\begin{aligned} 0 &= \rho_1\cos\phi_1(-\mu + a_1[3\rho_1^2 + x_2^2] + 3s_1^2 + y_2^2) \\ 0 &= x_2(-\mu + a_1[(2 - \cos 2\phi_1)\rho_1^2 + 3x_2^2] + s_1^2 + 3y_2^2) + 2\rho_1 s_1 y_2 \sin\phi_1 \sin\psi_1 \\ 0 &= s_1\cos\psi_1(-b\mu + 3\rho_1^2 + x_2^2 + a_2[3s_1^2 + y_2^2]) \\ 0 &= y_2(-b\mu + \rho_1^2 + 3x_2^2 + a_2[(2 - \cos 2\psi_1)s_1^2 + 3y_2^2]) + 2\rho_1 x_2 s_1 \sin\phi_1 \sin\psi_1. \end{aligned} \tag{2.20}$$

In order to construct solutions to Eq. (2.10) which are not covered via the symmetries by Lemma 2.1, one cannot choose the solution $\phi_1, \psi_1 = \pi/2 \pmod{\pi}$ in Eq. (2.19). First assume that

$$\phi_1, \psi_1 = 0 \pmod{\pi}. \tag{2.21}$$

Upon assuming that all of the variables will be nonzero Eq. (2.20) becomes

$$\begin{aligned}
0 &= -\mu + (3\rho_1^2 + x_2^2) + 3s_1^2 + y_2^2 \\
0 &= -\mu + a_1(\rho_1^2 + 3x_2^2) + s_1^2 + 3y_2^2 \\
0 &= -b\mu + 3\rho_1^2 + x_2^2 + a_2(3s_1^2 + y_2^2) \\
0 &= -b\mu + \rho_1^2 + 3x_2^2 + a_2(s_1^2 + 3y_2^2).
\end{aligned} \tag{2.22}$$

The solution to Eq. (2.22) is

$$\rho_1^2 = x_2^2 = \frac{a_2 - b}{4(a_1a_2 - 1)}\mu, \quad s_1^2 = y_2^2 = \frac{ba_1 - 1}{4(a_1a_2 - 1)}\mu. \tag{2.23}$$

Note that the restriction of Eq. (2.14) is valid for Eq. (2.23). Note that when $b = 1/a_1$ the solution is a vortex in the first component and identically zero in the second, whereas the situation is reversed at the limit $b = a_2$. This is the vortex-vortex solution.

Now consider Eq. (2.19) and Eq. (2.20) under the assumption that $\phi_1, \psi_1 = 0 \pmod{\pi}$ and $y_2 = 0$, i.e., the solution is real-valued in the second component. In this case the system to be solved for which all of the remaining variables are nonzero becomes

$$\begin{aligned}
0 &= -\mu + a_1(3\rho_1^2 + x_2^2) + 3s_1^2 \\
0 &= -\mu + a_1(\rho_1^2 + 3x_2^2) + s_1^2 \\
0 &= -b\mu + 3\rho_1^2 + x_2^2 + 3a_2s_1^2.
\end{aligned} \tag{2.24}$$

The solution to Eq. (2.24) is given by

$$\begin{pmatrix} \rho_1^2 \\ x_2^2 \\ s_1^2 \end{pmatrix} = \frac{\mu}{12a_1(a_1a_2 - 1)} \begin{pmatrix} 3a_1a_2 - 4ba_1 + 1 \\ 3(a_1a_2 - 1) \\ 4a_1(ba_1 - 1) \end{pmatrix}. \tag{2.25}$$

The solution is valid if and only if

$$\begin{aligned}
a_1a_2 > 1 &: 1/a_1 \le b \le (3a_1a_2 + 1)/4a_1 \\
a_1a_2 < 1 &: (3a_1a_2 + 1)/4a_1 \le b \le 1/a_1.
\end{aligned} \tag{2.26}$$

Note that in either case $\mu > 0$. Further note that if $b = 1/a_1$ corresponds to the solution with $q_2 \equiv 0$ and a vortex in q_1, and $b = (3a_1a_2+1)/4a_1$ corresponds to the solution described by Eq. (2.16), i.e., an out-of-phase dipole-dipole solution. This solution will be denoted by *azimuthon-dipole*, i.e., a phase-modulated vortex in the first component coupled to a dipole in the second component.

Finally consider Eq. (2.19) and Eq. (2.20) under the assumption that $\phi_1, \psi_1 = 0 \pmod{\pi}$ and $x_2 = 0$, i.e., the solution is real-valued in the first component. In this case the system to be solved for which all of the remaining variables are nonzero becomes

$$\begin{aligned}
0 &= -\mu + 3a_1\rho_1^2 + 3s_1^2 + y_2^2 \\
0 &= -b\mu + 3\rho_1^2 + a_2(3s_1^2 + y_2^2) \\
0 &= -b\mu + \rho_1^2 + a_2(s_1^2 + 3y_2^2).
\end{aligned} \tag{2.27}$$

The solution to Eq. (2.27) is given by

$$\begin{pmatrix} \rho_1^2 \\ s_1^2 \\ y_2^2 \end{pmatrix} = \frac{\mu}{12a_2(a_1a_2 - 1)} \begin{pmatrix} 4a_2(a_2 - b) \\ 3ba_1a_2 - 4a_2 + b \\ 3b(a_1a_2 - 1) \end{pmatrix}. \tag{2.28}$$

The solution is valid if and only if

$$\begin{aligned}
a_1a_2 > 1 &: a_2 \le b \le 4a_2/(3a_1a_2 + 1) \\
a_1a_2 < 1 &: 4a_2/(3a_1a_2 + 1) \le b \le a_2.
\end{aligned} \tag{2.29}$$

Again note that in either case $\mu > 0$. Furthermore, if $b = a_2$ corresponds to the solution with $q_1 \equiv 0$ and a vortex in q_2, and $b = 4a_2/(3a_1a_2+1)$ corresponds to the solution described by Eq. (2.16), i.e., an out-of-phase dipole-dipole solution. This solution will be denoted by *dipole-azimuthon*.

It is not difficult to show that any other solution to Eq. (2.10) which represents a solution which is complex-valued in at least one component is equivalent via the symmetries to those given above. In summary, the following result has now been proven.

Lemma 2.2. *The solution with a vortex in both components is given by*

$$q_1 \sim \sqrt{\frac{a_2 - b}{4(a_1a_2 - 1)g}\Delta\omega}\, q_{0,1}(r)\mathrm{e}^{\mathrm{i}\theta}, \quad q_2 \sim \sqrt{\frac{ba_1 - 1}{4(a_1a_2 - 1)g}\Delta\omega}\, q_{0,1}(r)\mathrm{e}^{\mathrm{i}\theta},$$

where $\Delta\omega > 0$. The restrictions on b are given in Eq. (2.14). The azimuthon-dipole solution is given by

$$\begin{aligned} q_1 &\sim q_{0,1}(r)\left(\sqrt{\frac{3a_1a_2 - 4ba_1 + 1}{12a_1(a_1a_2 - 1)g}\Delta\omega}\,\cos\theta + \mathrm{i}\sqrt{\frac{1}{4a_1g}\Delta\omega}\,\sin\theta\right) \\ q_2 &\sim q_{0,1}(r)\sqrt{\frac{ba_1 - 1}{3(a_1a_2 - 1)g}\Delta\omega}\,\cos\theta, \end{aligned}$$

where $\Delta\omega > 0$. The restrictions on b are given in Eq. (2.26). Finally, the dipole-azimuthon solution is given by

$$\begin{aligned} q_1 &\sim q_{0,1}(r)\sqrt{\frac{a_2 - b}{3(a_1a_2 - 1)g}\Delta\omega}\,\cos\theta \\ q_2 &\sim q_{0,1}(r)\left(\sqrt{\frac{3ba_1a_2 - 4a_2 + b}{12a_2(a_1a_2 - 1)g}\Delta\omega}\,\cos\theta + \mathrm{i}\sqrt{\frac{b}{4a_2g}\Delta\omega}\,\sin\theta\right), \end{aligned}$$

where $\Delta\omega > 0$. The restrictions on b are given in Eq. (2.29).

For $j = 1, 2$ the conserved quantities N_j (number of particles) are given by

$$N_j := \iint |q_j(x,t)|^2\,\mathrm{d}\boldsymbol{x}. \tag{2.30}$$

Let the ratio between these two quantities be defined by

$$R := \frac{N_1}{N_2} = \frac{|x_1|^2 + x_2^2}{|y_1|^2 + y_2^2} + \mathcal{O}(\epsilon). \tag{2.31}$$

The results of Lemma 2.1 and Lemma 2.2 are summarized in Figure 1. The horizontal axis is given by R. The labeling is such that "V" corresponds to vortex, "D" corresponds to dipole, and "A" corresponds to azimuthon. The subscript "i" means "in-phase", and the subscript "o" means "out-of-phase".

3. Stability: small eigenvalues

The theory leading to the determination of the spectral stability of the solutions found in Section 2 will heavily depend upon the results presented in [**25**, Section 4] and [**23**, **24**, **39**]. There are at least three conserved quantities associated with Eq. (1.3): two are given in Eq. (2.30), and the third is given by

$$L_z := \iint_{\mathbb{R}^2} \mathrm{Im}(q_j(\boldsymbol{x}))\partial_\theta\,\mathrm{Re}(q_j(\boldsymbol{x}))\,\mathrm{d}\boldsymbol{x}; \quad \partial_\theta := x\partial_y - y\partial_x,$$

where L_z refers to the total angular momentum of the condensate. Consequently, one typically has that $\lambda = 0$ is an eigenvalue with some multiplicity. When discussing the solutions given in Figure 1, one has the

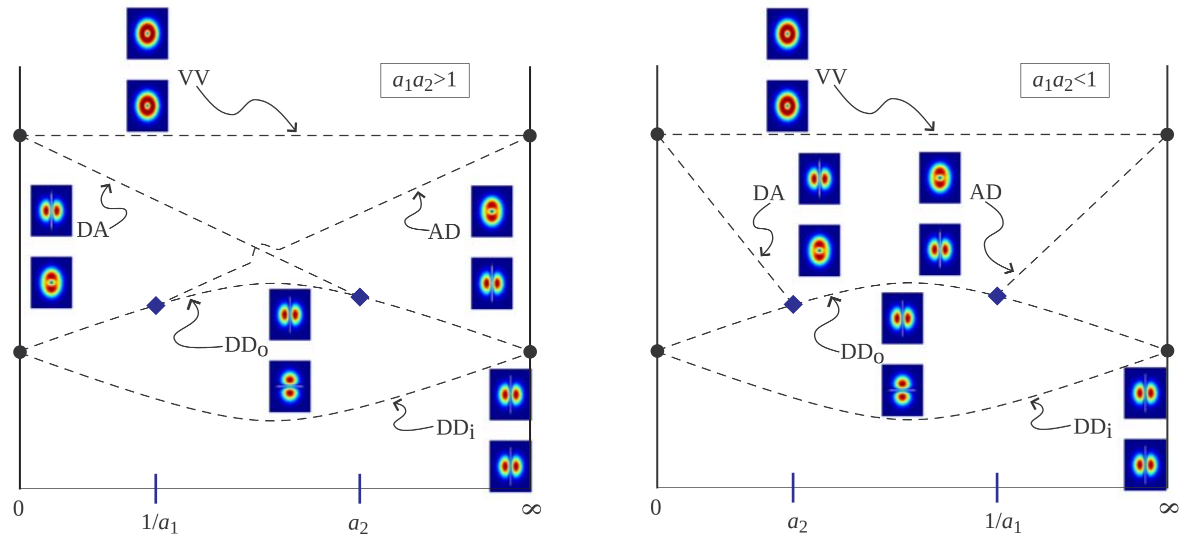

Figure 1: (color online) The existence diagram for the solutions discussed in Lemma 2.1 and Lemma 2.2. In each subfigure the horizontal axis is R as defined in Eq. (2.31). The labeling is such that "V" corresponds to vortex, "D" corresponds to dipole, and "A" corresponds to azimuthon. The subscript "i" means "in-phase", and the subscript "o" means "out-of-phase".

following table regarding the multiplicity of the null eigenvalue:

	$\mathrm{DD_i}$	$\mathrm{DD_o}$	DA	AD	VV
$m_{\mathrm{g}}(0)$	3	3	3	3	2
$m_{\mathrm{a}}(0)$	6	6	6	6	4

(3.1)

It is interesting to note that the vortex solutions VV do not have the maximal geometric multiplicity. The disparity when compared to the other solutions is due to the fact that the null eigenfunctions associated with N_j and L_z are constant multiples of each other for solutions of the form $q(r)\mathrm{e}^{\mathrm{i}\theta}$, i.e., solutions with radially symmetric moduli. The spectral stability results proven in the subsequent subsections are summarized in Figure 2.

3.1. Reduced eigenvalue problem: theory

A more complete version of the discussion in this subsection can be found in [**26**, Section 5.1]. It is given here for the sake of completeness. Upon linearizing Eq. (1.3) about a complex-valued solution one has the eigenvalue problem

$$\boldsymbol{J}\mathcal{L}\boldsymbol{u} = \lambda\boldsymbol{u}, \tag{3.2}$$

where

$$\boldsymbol{J} := \begin{pmatrix} 0 & \mathbb{1} \\ -\mathbb{1} & 0 \end{pmatrix},$$

and $\mathcal{L}$ is a symmetric operator on a Hilbert space X with inner product $\langle\cdot,\cdot\rangle$, and is a relatively compact perturbation of a self-adjoint and strictly positive operator. In particular, for $0 < \epsilon \ll 1$ consider Eq. (3.2)under the following scenario:

$$\mathcal{L} = \mathcal{L}_0 + \epsilon\mathcal{L}_1,$$

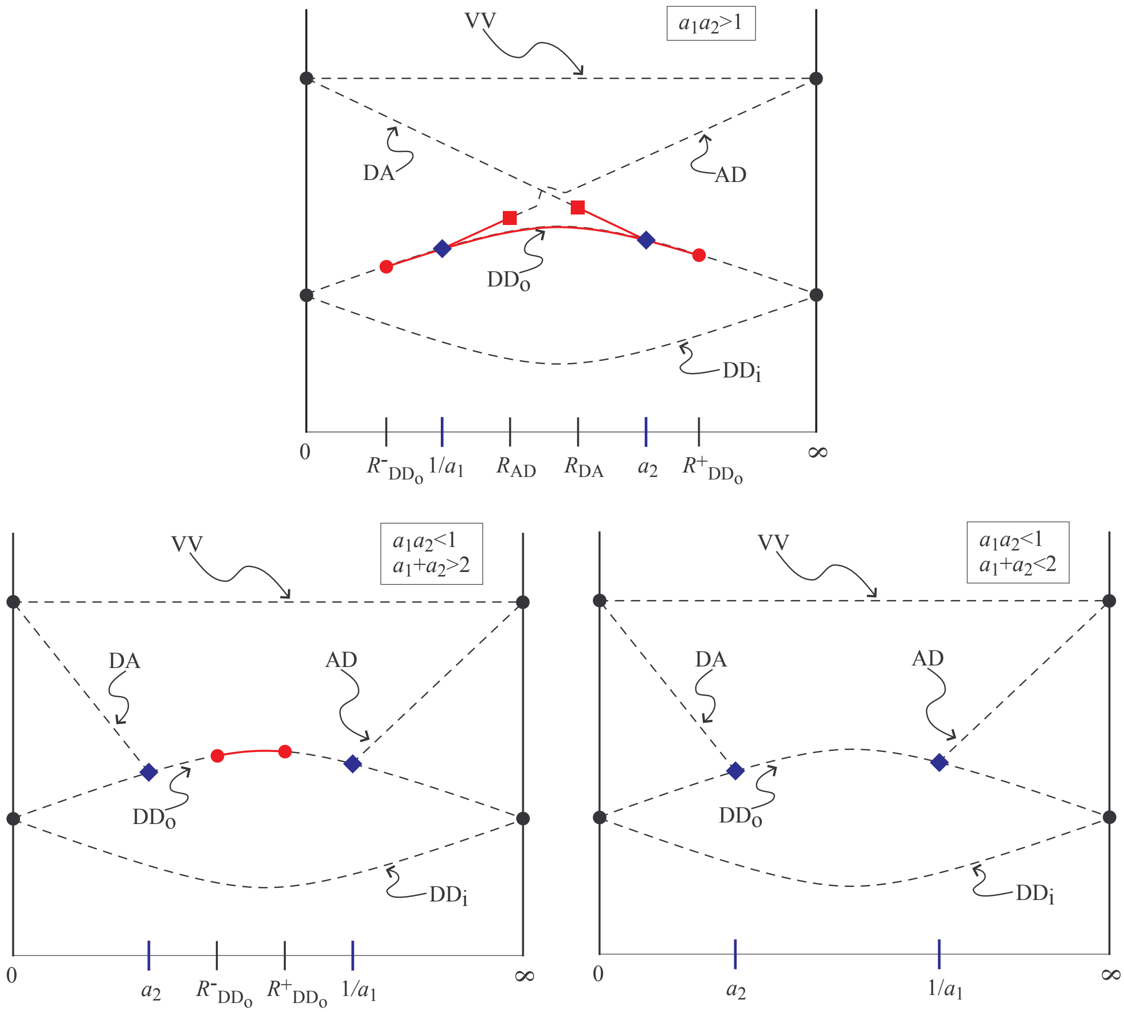

Figure 2: (color online) Recall the description associated with Figure 1. The solid red curve corresponds to solutions with one positive real eigenvalue. All other solutions have no purely real eigenvalues. The variables $R^{\pm}_{\mathrm{DD_o}}$ are defined in Eq. (3.12). The variables $R_{\mathrm{DA,AD}}$ are defined in Eq. (3.20) and Eq. (3.24), respectively.

with

$$\mathcal{L}_0 := \mathrm{diag}(\mathcal{A}_0, \mathcal{A}_0), \quad \mathcal{L}_1 := \begin{pmatrix} \mathcal{L}_+^1 & \mathcal{B} \\ \mathcal{B}^* & \mathcal{L}_-^1 \end{pmatrix}. \tag{3.3}$$

Assume that $\dim\ker(\mathcal{A}_0) = n \in \mathbb{N}$, and that an orthonormal basis for $\ker(\mathcal{A}_0)$ is given by

$$\ker(\mathcal{A}_0) = \mathrm{Span}\{\phi_1, \dots, \phi_n\}. \tag{3.4}$$

As seen in [**25**, Section 4], upon writing

$$\lambda = \epsilon\lambda_1 + \mathcal{O}(\epsilon^2), \quad u = \sum_{j=1}^{n} x_j(\phi_j, 0)^{\mathrm{T}} + \sum_{j=1}^{n} x_{n+j}(0, \phi_j)^{\mathrm{T}} + \mathcal{O}(\epsilon),$$

the determination of the $\mathcal{O}(\epsilon)$ eigenvalues to Eq. (3.3) is equivalent to the finite-dimensional eigenvalue problem

$$\boldsymbol{JSx} = \lambda_1\boldsymbol{x}; \quad \boldsymbol{J} := \begin{pmatrix} \boldsymbol{0} & \mathbb{1} \\ -\mathbb{1} & \boldsymbol{0} \end{pmatrix}, \ \boldsymbol{S} := \begin{pmatrix} \boldsymbol{S}_+ & \boldsymbol{S}_2 \\ \boldsymbol{S}_2^{\mathrm{H}} & \boldsymbol{S}_- \end{pmatrix}, \tag{3.5}$$

where $(\cdot)^{\mathrm{H}}$ is Hermitian conjugation and

$$(\boldsymbol{S}_{\pm})_{ij} = \langle \phi_i, \mathcal{L}_{\pm}^1 \phi_j \rangle, \quad (\boldsymbol{S}_2)_{ij} = \langle \phi_i, \mathcal{B}\phi_j \rangle. \tag{3.6}$$

3.2. Reduced eigenvalue problem: real-valued solutions

From the theory presented in Section 2 we can represent the steady-state solutions as $q_j = Q_j + \mathcal{O}(\epsilon)$, where Q_j is real-valued. Following the discussion of the previous subsection one has that $\mathcal{B} = 0$ with

$$\begin{aligned}\mathcal{L}_{+}^1 &= \begin{pmatrix} -\Delta\omega + 3a_1Q_1^2 + Q_2^2 & 2Q_1Q_2 \\ 2Q_1Q_2 & -b\Delta\omega + Q_1^2 + 3a_2Q_2^2 \end{pmatrix} \\ \mathcal{L}_{-}^1 &= \mathrm{diag}\left(-\Delta\omega + a_1Q_1^2 + Q_2^2, -b\Delta\omega + Q_1^2 + a_2Q_2^2\right).\end{aligned} \tag{3.7}$$

For $j = 1, 2$ write

$$\phi_{2j-1} := q_{0,1}(r)\cos\theta\, \boldsymbol{e}_j, \quad \phi_{2j} := q_{0,1}(r)\sin\theta\, \boldsymbol{e}_j,$$

where $\boldsymbol{e}_j \in \mathbb{R}^2$ is the standard unit basis vector. Recall from Eq. (3.1) that there will be only one pair of $\mathcal{O}(\epsilon)$ nonzero eigenvalues when solving Eq. (3.5).

3.2.1. In-phase dipole-dipole

Upon using Eq. (2.13) and Eq. (3.6) one eventually sees that

$$\begin{aligned}\boldsymbol{S}_{+} &= 2g\begin{pmatrix} 3a_1x_1^2 & 0 & 3x_1y_1 & 0 \\ 0 & -y_1^2 & 0 & x_1y_1 \\ 3x_1y_1 & 0 & 3a_2y_1^2 & 0 \\ 0 & x_1y_1 & 0 & -x_1^2 \end{pmatrix} \\ \boldsymbol{S}_{-} &= -2g\,\mathrm{diag}\left(0, a_1x_1^2 + y_1^2, 0, x_1^2 + a_2y_1^2\right).\end{aligned} \tag{3.8}$$

From Eq. (3.5) it is seen that the nonzero eigenvalues are given by

$$\lambda_1^2 = -4g^2\left[x_1^2(x_1^2 + a_2y_1^2) + y_1^2(a_1x_1^2 + y_1^2)\right] \in \mathbb{R}^-; \tag{3.9}$$

hence, these waves are spectrally stable with respect to small eigenvalues.

3.2.2. Out-of-phase dipole-dipole

From Eq. (2.16) and Eq. (3.6) one gets that

$$\begin{aligned}\boldsymbol{S}_{+} &= 2g\begin{pmatrix} 3a_1\rho_1^2 & 0 & 0 & \rho_1y_2 \\ 0 & y_2^2 & \rho_1y_2 & 0 \\ 0 & \rho_1y_2 & \rho_1^2 & 0 \\ \rho_1y_2 & 0 & 0 & 3a_2y_2^2 \end{pmatrix} \\ \boldsymbol{S}_{-} &= 2g\,\mathrm{diag}\left(0, -a_1\rho_1^2 + y_2^2, \rho_1^2 - a_2y_2^2, 0\right).\end{aligned} \tag{3.10}$$

Note that

$$-a_1\rho_1^2 + y_2^2 = 0 \quad \Longrightarrow \quad R = 1/a_1,$$

and

$$\rho_1^2 - a_2y_2^2 = 0 \quad \Longrightarrow \quad R = a_2,$$

where R is defined in Eq. (2.31). Thus, it is seen that the bifurcation from $\mathrm{DD_o}$ to AD or DA is realized spectrally as an eigenvalue of L_- passing through the origin. Using Eq. (3.5) it is seen that the nonzero eigenvalues are given by

$$\lambda_1^2 = -4g^2\left[x_1^2(\rho_1^2 - a_2y_2^2) + y_1^2(-a_1\rho_1^2 + y_2^2)\right]. \tag{3.11}$$

If one sets

$$R^{\pm}_{\mathrm{DD_o}} := \frac{1}{2}\left(a_1 + a_2 \pm \sqrt{(a_1+a_2)^2 - 4}\right), \tag{3.12}$$

then an analysis of Eq. (3.11) yields

$$\lambda_1^2 > 0 \quad\Longleftrightarrow\quad R^{-}_{\mathrm{DD_o}} < \frac{\rho_1^2}{y_2^2} < R^{+}_{\mathrm{DD_o}}; \tag{3.13}$$

otherwise, $\lambda_1^2 < 0$. In conclusion, the real eigenvalues of $\mathcal{O}(\epsilon)$ can exist only if $a_1 + a_2 > 2$.

3.3. Reduced eigenvalue problem: complex-valued solutions

If the underlying solution is written as $q_j = U_j + \mathrm{i}V_j$ for $j = 1, 2$, then in this case one has that

$$\begin{aligned}
\mathcal{L}^1_+ &= \begin{pmatrix} -\Delta\omega + a_1(3U_1^2 + V_1^2) + U_2^2 + V_2^2 & 2U_1U_2 \\ 2U_1U_2 & -b\Delta\omega + U_1^2 + V_1^2 + a_2(3U_2^2 + V_2^2) \end{pmatrix} \\
\mathcal{L}^1_- &= \begin{pmatrix} -\Delta\omega + a_1(U_1^2 + 3V_1^2) + U_2^2 + V_2^2 & 2V_1V_2 \\ 2V_1V_2 & -b\Delta\omega + U_1^2 + V_1^2 + a_2(U_2^2 + 3V_2^2) \end{pmatrix} \\
\mathcal{B} &= 2\begin{pmatrix} a_1U_1V_1 & U_1V_2 \\ U_2V_1 & a_2U_2V_2 \end{pmatrix}.
\end{aligned} \tag{3.14}$$

3.3.1. Vortex-vortex

Upon using Eq. (2.23) and Eq. (3.6) one has

$$\begin{aligned}
\boldsymbol{S}_+ = 2g\begin{pmatrix} 3a_1\rho_1^2 & 0 & 3\rho_1 s_1 & 0 \\ 0 & a_1\rho_1^2 & 0 & \rho_1 s_1 \\ 3\rho_1 s_1 & 0 & 3a_2 s_1^2 & 0 \\ 0 & \rho_1 s_1 & 0 & a_2 s_1^2 \end{pmatrix}, \quad
\boldsymbol{S}_- = 2g\begin{pmatrix} a_1\rho_1^2 & 0 & \rho_1 s_1 & 0 \\ 0 & 3a_1\rho_1^2 & 0 & 3\rho_1 s_1 \\ \rho_1 s_1 & 0 & a_2 s_1^2 & 0 \\ 0 & 3\rho_1 s_1 & 0 & 3a_2 s_1^2 \end{pmatrix} \\
\boldsymbol{S}_2 = 2g\begin{pmatrix} 0 & a_1\rho_1^2 & 0 & \rho_1 s_1 \\ a_1\rho_1^2 & 0 & \rho_1 s_1 & 0 \\ 0 & \rho_1 s_1 & 0 & a_2 s_1^2 \\ \rho_1 s_1 & 0 & a_2 s_1^2 & 0 \end{pmatrix}.
\end{aligned} \tag{3.15}$$

From Eq. (3.5) it is seen that the nonzero eigenvalues represented by $Z := \lambda_1/2g$ satisfy the characteristic equation

$$Z^4 + 4(a_1^2\rho_1^4 + 2\rho_1^2 s_1^2 + a_2^2 s_1^4)Z^2 + 16(a_1a_2 - 1)^2\rho_1^4 s_1^4 = 0. \tag{3.16}$$

Now, one can rewrite the above as

$$\left[Z^2 + 2(a_1^2\rho_1^4 + 2\rho_1^2 s_1^2 + a_2^2 s_1^4)\right]^2 + 16(a_1a_2 - 1)^2\rho_1^4 s_1^4 - 4(a_1^2\rho_1^4 + 2\rho_1^2 s_1^2 + a_2^2 s_1^4)^2 = 0.$$

Upon using Eq. (2.23) and simplifying one gets that

$$16(a_1a_2 - 1)^2\rho_1^4 s_1^4 - 4(a_1^2\rho_1^4 + 2\rho_1^2 s_1^2 + a_2^2 s_1^4)^2 = -\left(\frac{a_1(a_2 - b) - a_2(ba_1 - 1)}{a_1a_2 - 1}\right)^2;$$

hence, for Eq. (3.16) solutions $\hat{Z}$ satisfy $\hat{Z}^2 \in \mathbb{R}^-$. Since

$$a_1^2\rho_1^4 + 2\rho_1^2 s_1^2 + a_2^2 s_1^4 > 0,$$

one has that all of the solutions must be simple zeros; consequently, the solution is spectrally stable with respect to the small eigenvalues.

3.3.2. Azimuthon-dipole

Upon using Eq. (2.25) and Eq. (3.6) one gets

$$\boldsymbol{S}_+ = 2g\begin{pmatrix} 3a_1\rho_1^2 & 0 & 3\rho_1 s_1 & 0 \\ 0 & a_1\rho_1^2 & 0 & \rho_1 s_1 \\ 3\rho_1 s_1 & 0 & 3a_2 s_1^2 & 0 \\ 0 & \rho_1 s_1 & 0 & x_2^2-\rho_1^2 \end{pmatrix}, \quad \boldsymbol{S}_- = 2g\begin{pmatrix} a_1 x_2^2 & 0 & 0 & 0 \\ 0 & 3a_1x_2^2 & 0 & 0 \\ 0 & 0 & 0 & 0 \\ 0 & 0 & 0 & -\rho_1^2+x_2^2-a_2s_1^2 \end{pmatrix}$$
$$\boldsymbol{S}_2 = 2g\begin{pmatrix} 0 & a_1\rho_1x_2 & 0 & 0 \\ a_1\rho_1x_2 & 0 & 0 & 0 \\ 0 & s_1x_2 & 0 & 0 \\ s_1x_2 & 0 & 0 & 0 \end{pmatrix}. \tag{3.17}$$

Since

$$-\rho_1^2+x_2^2 = s_1^2/a_1, \quad -\rho_1^2+x_2^2-a_2s_1^2 = -4(ba_1-1)/3,$$

upon using Eq. (3.5) it is seen that the nonzero eigenvalues satisfy

$$\left(\frac{\lambda_1}{2g}\right)^2 = \frac{4x_2^2}{3a_1}\left[-3a_1^3\rho_1^2+(ba_1-1)s_1^2\right]. \tag{3.18}$$

Upon using the expressions given in Eq. (2.25) it can be seen that $\lambda_1 = 0$ if and only if $b = b_\pm$, where

$$b_\pm := \frac{1}{a_1} + \frac{3}{2}a_1\left(-1 \pm \sqrt{1+(a_1a_1-1)/a_1^2}\right). \tag{3.19}$$

It is an exercise in algebra to check that

$$b_- - \frac{1}{a_1} < 0, \quad b_\pm - \frac{1+3a_1a_2}{4a_1} < 0, \quad b_+ - \frac{1}{a_1}\begin{cases} > 0, & a_1a_2 > 1 \\ < 0, & a_1a_2 < 1. \end{cases}$$

Set

$$R_{\mathrm{AD}} := \left.\frac{\rho_1^2+x_2^2}{s_1^2}\right|_{b=b_+}, \tag{3.20}$$

where b_+ is defined in Eq. (3.19). If $a_1a_2 > 1$, then one can conclude that for Eq. (3.18) $\lambda_1^2 > 0$ for $1/a_1 \le R < R_{\mathrm{AD}}$; otherwise, $\lambda_1^2 < 0$. Consequently, there is a pair of small real eigenvalues for $1/a_1 \le R < R_{\mathrm{AD}}$, and otherwise the small eigenvalues are purely imaginary. If $a_1a_2 < 1$, $\lambda_1^2 < 0$, so that the eigenvalues are always purely imaginary (see Figure 2).

3.3.3. Dipole-azimuthon

Using Eq. (2.28) and Eq. (3.6) yields

$$\boldsymbol{S}_+ = 2g\begin{pmatrix} 3a_1\rho_1^2 & 0 & 3\rho_1 s_1 & 0 \\ 0 & -s_1^2+y_2^2 & 0 & \rho_1 s_1 \\ 3\rho_1 s_1 & 0 & 3a_2 s_1^2 & 0 \\ 0 & \rho_1 s_1 & 0 & a_2s_1^2 \end{pmatrix}, \quad \boldsymbol{S}_- = 2g\begin{pmatrix} 0 & 0 & 0 & 0 \\ 0 & a_1\rho_1^2-s_1^2+y_2^2 & 0 & 0 \\ 0 & 0 & a_2y_2^2 & 0 \\ 0 & 0 & 0 & 3a_2y_2^2 \end{pmatrix}$$
$$\boldsymbol{S}_2 = 2g\begin{pmatrix} 0 & a_2s_1y_2 & 0 & 0 \\ a_2s_1y_2 & 0 & 0 & 0 \\ 0 & \rho_1y_2 & 0 & 0 \\ \rho_1y_2 & 0 & 0 & 0 \end{pmatrix}. \tag{3.21}$$

Since

$$-s_1^2+y_2^2 = \rho_1^2/a_2, \quad a_1\rho_1^2-s_1^2+y_2^2 = -4(a_2-b)/3b,$$

by using Eq. (3.5) it is eventually seen that the nonzero eigenvalues are given by

$$\left(\frac{\lambda_1}{2g}\right)^2 = \frac{4y_2^2}{3ba_2}\left[(a_2-b)\rho_1^2 - 3ba_2^3s_1^2\right]. \tag{3.22}$$

Using the expressions given in Eq. (2.28) yields that $\lambda_1 = 0$ if and only if $b = b_\pm$, where now

$$b_\pm := \frac{4a_2}{3a_2^2(3a_1a_2+1)-4}\left(-1+\frac{3}{2}a_2^2\left[1\pm\sqrt{1+(a_1a_1-1)/a_2^2}\right]\right). \tag{3.23}$$

Arguing as in the previous subsection it can eventually be seen that for

$$R_{\mathrm{DA}} := \left.\frac{\rho_1^2}{s_1^2+y_2^2}\right|_{b=b_+}, \tag{3.24}$$

where b_+ is defined in Eq. (3.23), if $a_1a_2 > 1$, then $\lambda_1^2 > 0$ for $R_{\mathrm{DA}} \le R < a_2$; otherwise, $\lambda_1^2 < 0$. Consequently, there is a pair of small real eigenvalues for $R_{\mathrm{DA}} \le R < a_2$, and otherwise the small eigenvalues are purely imaginary. If $a_1a_2 < 1$, $\lambda_1^2 < 0$, so that the eigenvalues are always purely imaginary (see Figure 2).

4. Stability: Hamiltonian-Hopf bifurcations

In the previous sections the $\mathcal{O}(\epsilon)$ eigenvalues were determined. Herein we will locate the potentially unstable $\mathcal{O}(1)$ eigenvalues which arise from a Hamiltonian-Hopf bifurcation. This bifurcation is possible only if for the unperturbed problem there is the collision of eigenvalues of opposite sign, i.e., only for the eigenvalues $\pm\mathrm{i}2$. A preliminary theoretical result, derived in [**26**, Section 6.1], will be needed before the actual calculations are presented. In particular, we first consider the nongeneric case for which the eigenvalue is algebraically simple.

4.1. *Reduced eigenvalue problem: theory*

A more complete version of the discussion in this subsection can be found in [**26**, Section 6.1]. As in Section 3.1, it is given here for the sake of completeness. Consider the scenario presented in Section 3.1. First suppose that $\epsilon = 0$. Let $\lambda^\pm \in \sigma(\mathcal{L}) \cap \mathbb{R}^\pm$ each be semi-simple eigenvalues with multiplicity $n_\pm$; furthermore, let the basis of each eigenspace be given by the orthonormal set $\{\psi_1^\pm, \dots, \psi_{n_\pm}^\pm\}$. When considering only those eigenvalues in the upper-half of the complex plane, for Eq. (3.2) the eigenvalues and corresponding eigenfunctions are given by

$$\begin{aligned} \lambda = -\mathrm{i}\lambda^- : \quad & u_j^- = (\psi_j^-, -\mathrm{i}\psi_j^-)^{\mathrm{T}},\ j = 1,\dots n_- \\ \lambda = +\mathrm{i}\lambda^+ : \quad & u_j^+ = (\psi_j^+, \mathrm{i}\psi_j^+)^{\mathrm{T}},\ j = 1,\dots n_+. \end{aligned} \tag{4.1}$$

If one assumes that $\lambda^- = -\lambda^+$, then there is a collision of eigenvalues with opposite Krein signature; in particular, n_- eigenvalues of negative sign have collided with n_+ eigenvalues of positive sign. Under this scenario the eigenspace associated with the colliding eigenvalues is also *semi-simple*. As discussed in [**32**], this is a codimension three phenomenon, and hence is nongeneric.

The location of the perturbed eigenvalues can be found in the following manner. First write the perturbed eigenvalue and eigenfunction using the expansion

$$\lambda = \mathrm{i}\lambda^+ + \epsilon\lambda_1 + \mathcal{O}(\epsilon^2), \quad u = \sum_{j=1}^{n_-} c_j^- u_j^- + \sum_{j=1}^{n_+} c_j^+ u_j^+ + \mathcal{O}(\epsilon), \tag{4.2}$$

and set $\boldsymbol{c} := (c_1^-, \dots, c_{n_-}^-, c_1^+, \dots, c_{n_+}^+)^{\mathrm{T}} \in \mathbb{C}^{n_-+n_+}$. One eventually sees that the $\mathcal{O}(\epsilon)$ correction is found by solving the matrix system

$$\boldsymbol{J}\boldsymbol{S}\boldsymbol{c} = \lambda_1\boldsymbol{c}; \quad \boldsymbol{J} := -\frac{\mathrm{i}}{2}\,\mathrm{diag}(\mathbb{1}_-, -\mathbb{1}_+), \quad \boldsymbol{S} := \begin{pmatrix} \boldsymbol{S}_- & \boldsymbol{S}_{\mathrm{c}} \\ \boldsymbol{S}_{\mathrm{c}}^{\mathrm{H}} & \boldsymbol{S}_+ \end{pmatrix}, \tag{4.3}$$

where

$$(\boldsymbol{S}_\pm)_{jk} = \langle(\mathcal{L}_+^1 + \mathcal{L}_-^1)\psi_j^\pm, \psi_k^\pm\rangle, \quad (\boldsymbol{S}_\mathrm{c})_{jk} = \langle(\mathcal{L}_+^1 - \mathcal{L}_-^1 + \mathrm{i}2\mathcal{B})\psi_j^-, \psi_k^+\rangle. \tag{4.4}$$

In Eq. (4.3) one has that $\mathbb{1}_\pm \in \mathbb{R}^{n_\pm \times n_\pm}$ is the identity matrix. Note that $\boldsymbol{J}$ is skew-symmetric and that $\boldsymbol{S}$ is symmetric.

Remark 4.1. As a consequence of theoretical results presented in [**22**, Section 2] (also see the references therein) it is known regarding Eq. (4.3) that

- $\{\lambda, -\overline{\lambda}\} \subset \sigma(\boldsymbol{J}\boldsymbol{S})$
- the number of $\lambda \in \sigma(\boldsymbol{J}\boldsymbol{S})$ with $\operatorname{Re}\lambda \neq 0$ is bounded above by $\min\{n_-, n_+\}$.

Let us now apply these results to those solutions found in Section 2. Recall that from Section 2 the solutions bifurcate from $\lambda = 4$. When $\epsilon = 0$ the eigenvalue $\lambda_{m,\ell}$ maps to $\pm\mathrm{i}(4 - \lambda_{m,\ell})$. Thus, upon following the ideas presented in Section 4.1 one knows that a Hamiltonian-Hopf bifurcation will be associated with those eigenvalues which satisfy

$$4 - \lambda_{a,b} = \lambda_{c,d} - 4; \quad \lambda_{a,b} \in \sigma(\mathcal{L}) \cap \mathbb{R}^-,\ \lambda_{c,d} \in \sigma(\mathcal{L}) \cap \mathbb{R}^+.$$

A simple calculation shows that the above is satisfied if and only if

$$(a, b) = (0, 0): \quad (c, d) \in \{(0, 2), (1, 0)\}. \tag{4.5}$$

As a consequence, in the upper-half of the complex plane one has one distinct possible bifurcation point at i2. Furthermore, $n_- = 2$ and $n_+ = 6$, so that there will be at most two eigenvalues with real part nonzero for $\epsilon > 0$. Using the notation leading to Eq. (4.1) one has that

$$\begin{aligned}
&\psi_j^- = q_{0,0}(r)\boldsymbol{e}_j, \quad j = 1, 2\\
&\psi_1^+ = q_{1,0}(r)\boldsymbol{e}_1,\ \psi_2^+ = q_{0,2}(r)\cos 2\theta\,\boldsymbol{e}_1,\ \psi_3^+ = q_{0,2}(r)\sin 2\theta\,\boldsymbol{e}_1\\
&\psi_4^+ = q_{1,0}(r)\boldsymbol{e}_1,\ \psi_5^+ = q_{0,2}(r)\cos 2\theta\,\boldsymbol{e}_2,\ \psi_6^+ = q_{0,2}(r)\sin 2\theta\,\boldsymbol{e}_2.
\end{aligned} \tag{4.6}$$

The functions are explicitly given by

$$q_{0,0}(r) = \sqrt{\frac{1}{\pi}}\,\mathrm{e}^{-r^2/2};\ q_{1,0}(r) = \sqrt{\frac{1}{\pi}}\,(1 - r^2)\mathrm{e}^{-r^2/2};\ q_{0,\ell}(r) = \sqrt{\frac{2}{\ell!\pi}}\,r^\ell \mathrm{e}^{-r^2/2},\ \ell \in \mathbb{N}. \tag{4.7}$$

Finally, regarding Eq. (4.3) one has that the operators $\mathcal{L}_\pm^1$ and $\mathcal{B}$ are given in Eq. (3.7). Since $\boldsymbol{J}, \boldsymbol{S} \in \mathbb{C}^{8\times 8}$, Eq. (4.3) unfortunately is in general not analytically tractable. However, it turns out to be the case that at the limits $R = 0, \infty$ (see Figure 1) one can perform a perturbation analysis of the characteristic equation in order to determine if an instability is generated near those limits. Otherwise, the eigenvalues in Eq. (4.3) can be determined numerically.

4.2. Reduced eigenvalue problem: real-valued solutions

4.2.1. In-phase dipole-dipole

For this problem $\mathcal{B} = 0$ and

$$\begin{aligned}
\mathcal{L}_+^1 - \mathcal{L}_-^1 &= q_{0,1}^2(r)(1 + \cos 2\theta)\begin{pmatrix} a_1 x_1^2 & x_1 y_1 \\ x_1 y_1 & a_2 y_1^2 \end{pmatrix}\\
\mathcal{L}_+^1 + \mathcal{L}_-^1 &= -2\Delta\omega\,\mathrm{diag}(1, b) + q_{0,1}^2(r)(1 + \cos 2\theta)\begin{pmatrix} 2a_1 x_1^2 + y_1^2 & x_1 y_1 \\ x_1 y_1 & x_1^2 + 2a_2 y_1^2 \end{pmatrix}.
\end{aligned}$$

In using Eq. (4.3) along with the expressions in Eq. (2.13) and Eq. (4.7) it is seen that

$$\boldsymbol{S}_\mathrm{c} = 2g\begin{pmatrix} 0 & a_1 x_1^2 & 0 & 0 & x_1 y_1 & 0 \\ 0 & x_1 y_1 & 0 & 0 & a_2 y_1^2 & 0 \end{pmatrix}, \quad \boldsymbol{S}_- = 2g\begin{pmatrix} a_1 x_1^2 - y_1^2 & 2x_1 y_1 \\ 2x_1 y_1 & -x_1^2 + a_2 y_1^2 \end{pmatrix},$$

and

$$\boldsymbol{S}_+ = 2g\begin{pmatrix} -(a_1x_1^2+2y_1^2) & -(a_1x_1^2+y_1^2/2) & 0 & x_1y_1 & -x_1y_1/2 & 0 \\ -(a_1x_1^2+y_1^2/2) & -3y_1^2/2 & 0 & -x_1y_1/2 & 3x_1y_1/2 & 0 \\ 0 & 0 & -3y_1^2/2 & 0 & 0 & 3x_1y_1/2 \\ x_1y_1 & -x_1y_1/2 & 0 & -(2x_1^2+a_2y_1^2) & -(x_1^2/2+a_2y_1^2) & 0 \\ -x_1y_1/2 & 3x_1y_1/2 & 0 & -(x_1^2/2+a_2y_1^2) & -3x_1^2/2 & 0 \\ 0 & 0 & 3x_1y_1/2 & 0 & 0 & -3x_1^2/2 \end{pmatrix}.$$

When considering Eq. (4.3) at the limits $b = 1/a_1, a_2$ one has the semisimple eigenvalues

$$b = 1/a_1 : \ \mathrm{i}\frac{\lambda_1}{g} = \frac{1}{3}; \quad b = a_2 : \ \mathrm{i}\frac{\lambda_1}{g} = \frac{a_2}{3}.$$

All of the other eigenvalues are simple with zero real part; hence, for small perturbations they will remain purely imaginary. A Taylor expansion of the characteristic equation yields to leading order

$$b = 1/a_1 : \ \left(\mathrm{i}\frac{\lambda_1}{g} - \frac{1}{3}\right)^2 - \frac{a_1(a_1-1)^2(12a_1-17)}{9(a_1+1)(a_1a_2-1)(4a_1^2-14a_1+11)}\left(b - \frac{1}{a_1}\right) = 0, \tag{4.8}$$

and

$$b = a_2 : \ \left(\mathrm{i}\frac{\lambda_1}{g} - \frac{a_2}{3}\right)^2 + \frac{a_2(a_2-1)^2(12a_2-17)}{9(a_2+1)(a_1a_2-1)(4a_2^2-14a_2+11)}(b - a_2) = 0. \tag{4.9}$$

Set

$$a_\pm := \frac{1}{4}(7 \pm \sqrt{5}) \quad (a_- \sim 1.19,\ a_+ \sim 2.31).$$

First suppose that $a_1a_2 > 1$, so that $1/a_1 < b < a_2$. From Eq. (4.8) it is seen that $\mathrm{Re}\,\lambda_1 \neq 0$ if $a_1 < a_-$ or $17/12 < a_1 < a_+$, and $\mathrm{Re}\,\lambda_1 = 0$ for complementary values of a_1. One sees the same situation arising from the analysis of Eq. (4.9), i.e., $\mathrm{Re}\,\lambda_1 \neq 0$ if and only if $a_2 < a_-$ or $17/12 < a_2 < a_+$. On the other hand, if $a_1a_2 < 1$ then an instability arises near $b = 1/a_1$ if and only if $a_- < a_1 < 17/12$ or $a_+ < a_1$, and an instability arises near $b = a_2$ if and only if $a_- < a_2 < 17/12$ or $a_+ < a_2$. The situation is depicted in Figure 3.

We numerically compute $\mathrm{Re}\,\lambda_1$ for the relevant experimental parameters $(a_1, a_2) = (1.03, 0.9717)$ in the left panel of Figure 4. As predicted by the theory, the solution undergoes the Hamiltonian-Hopf bifurcation near the limits $0 < b - 1/a_1 \ll 1$ and $0 < a_2 - b \ll 1$. It is seen in the figure that the bifurcation occurs for all values of b.

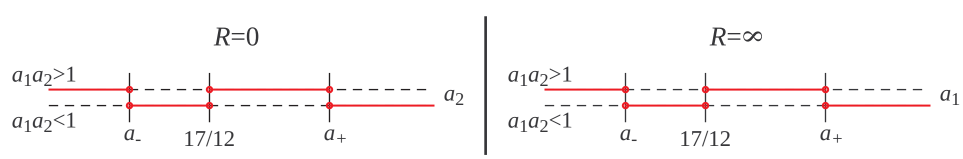

Figure 3: (color online) Regarding the solution $\mathrm{DD_i}$, the left panel is concerned with Hamiltonian-Hopf bifurcations near $R = 0$, whereas the right panel is concerned with such bifurcations near $R = \infty$. The horizontal axis is a_2 on the left and a_1 on the right. The solid red curve corresponds to the bifurcation occurring; otherwise, the bifurcation does not occur.

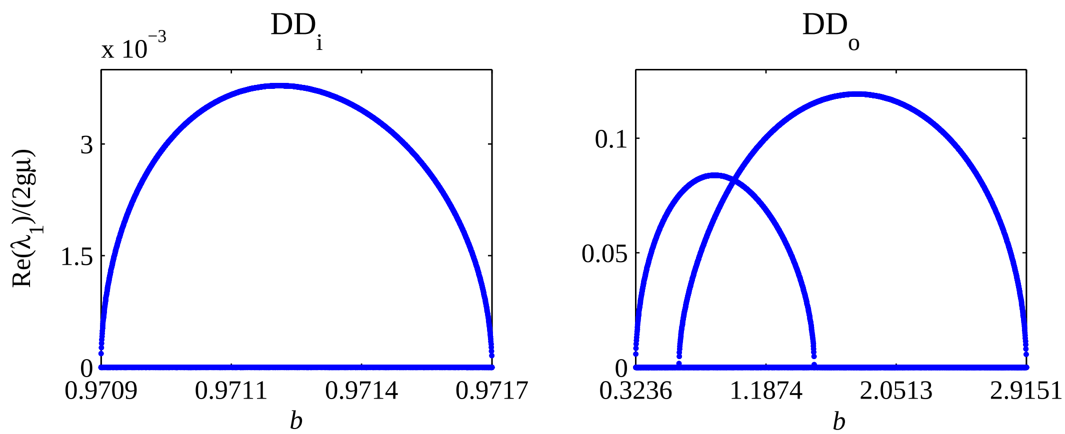

Figure 4: (color online) Numerically computed $\mathrm{Re}\,\lambda_1$ from the reduced eigenvalue problem Eq. (4.3) for the relevant experimental parameters $(a_1, a_2) = (1.03, 0.9717)$. The left panel shows the results of the computation for the solution $\mathrm{DD_i}$, and therefore has $b \in (1/a_1, a_2)$, while the right panel shows the results for the solution $\mathrm{DD_o}$, so that $b \in (1/3a_1, 3a_2)$.

4.2.2. Out-of-phase dipole-dipole

For this problem $\mathcal{B} = 0$ and

$$\begin{aligned}
\mathcal{L}_+^1 - \mathcal{L}_-^1 &= q_{0,1}^2(r)\begin{pmatrix} a_1x_1^2(1+\cos 2\theta) & x_1y_2\sin 2\theta \\ x_1y_2\sin 2\theta & a_2y_2^2(1-\cos 2\theta)\end{pmatrix} \\
\mathcal{L}_+^1 + \mathcal{L}_-^1 &= -2\Delta\omega\,\mathrm{diag}(1,b) + q_{0,1}^2(r)\begin{pmatrix} 2a_1(1+\cos 2\theta)x_1^2 + (1-\cos 2\theta)y_2^2 & x_1y_2\sin 2\theta \\ x_1y_2\sin 2\theta & (1+\cos 2\theta)x_1^2 + 2a_2(1-\cos 2\theta)y_2^2\end{pmatrix}.
\end{aligned}$$

In using Eq. (4.3) along with the expressions in Eq. (2.16) and Eq. (4.7) it is eventually seen that

$$\boldsymbol{S}_{\mathrm{c}} = 2g\begin{pmatrix} 0 & a_1x_1^2 & 0 & 0 & 0 & x_1y_2 \\ 0 & 0 & x_1y_2 & 0 & -a_2y_2^2 & 0\end{pmatrix}, \quad \boldsymbol{S}_- = 2g\begin{pmatrix} a_1x_1^2 + y_2^2 & 0 \\ 0 & x_1^2 + a_2y_2^2\end{pmatrix},$$

and

$$\boldsymbol{S}_+ = 2g\begin{pmatrix} -a_1x_1^2 & -a_1x_1^2 + y_2^2/2 & 0 & 0 & 0 & -x_1y_2/2 \\ -a_1x_1^2 + y_2^2/2 & y_2^2/2 & 0 & 0 & 0 & 0 \\ 0 & 0 & y_2^2/2 & -x_1y_2/2 & 0 & 0 \\ 0 & 0 & -x_1y_2/2 & -a_2y_2^2 & -x_1^2/2 + a_2y_2^2 & 0 \\ 0 & 0 & 0 & -x_1^2/2 + a_2y_2^2 & x_1^2/2 & 0 \\ -x_1y_2/2 & 0 & 0 & 0 & 0 & x_1^2/2\end{pmatrix}.$$

When considering Eq. (4.3) at the limits $b = 1/3a_1, 3a_2$ one has the semisimple eigenvalues

$$b = 1/3a_1:\ \mathrm{i}\frac{\lambda_1}{g} = \frac{1}{3}; \quad b = 3a_2:\ \mathrm{i}\frac{\lambda_1}{g} = a_2.$$

All of the other eigenvalues are simple with zero real part; hence, for small perturbations they will remain purely imaginary. A Taylor expansion of the characteristic equation yields to leading order

$$b = 1/3a_1:\ \left(\mathrm{i}\frac{\lambda_1}{g} - \frac{1}{3}\right)^2 + \frac{a_1(4a_1+1)}{2(2a_1+1)(9a_1a_2-1)}\left(b - \frac{1}{3a_1}\right) = 0, \tag{4.10}$$

and

$$b = 3a_2:\ \left(\mathrm{i}\frac{\lambda_1}{g} - a_2\right)^2 - \frac{a_2(4a_2+1)}{2(2a_2+1)(9a_1a_2-1)}(b - 3a_2) = 0. \tag{4.11}$$

An analysis of Eq. (4.10) and Eq. (4.11) yields that $\mathrm{Re}\,\lambda_1 \neq 0$ for both $9a_1a_2 > 1$ and $9a_1a_2 < 1$ near the two limits; in other words, there is a Hamiltonian-Hopf bifurcation at both limits.

We numerically compute $\mathrm{Re}\,\lambda_1$ for the relevant experimental parameters $(a_1, a_2) = (1.03, 0.9717)$ in the right panel of Figure 4. As predicted by the theory, the solution undergoes the Hamiltonian-Hopf bifurcation near the limits $0 < b - 1/3a_1 \ll 1$ and $0 < 3a_2 - b \ll 1$. It is seen in the figure that the bifurcation occurs for all values of b. Furthermore, there is a range of b values for which two eigenvalues with positive real part arise as a consequence of the bifurcation.

4.3. Reduced eigenvalue problem: complex-valued solutions

Herein the analysis will be done for only the solution VV. The analysis for the other two solutions is left for the interested reader.

4.3.1. Vortex-vortex

Regarding Eq. (4.3) one has that the operators $\mathcal{L}_\pm^1$ and $\mathcal{B}$ are given in Eq. (3.14). For this problem one then has that

$$\mathcal{L}_+^1 - \mathcal{L}_-^1 + \mathrm{i}2\mathcal{B} = 2q_{0,1}^2(r)\mathrm{e}^{\mathrm{i}2\theta}\begin{pmatrix} a_1\rho_1^2 & \rho_1 s_1 \\ \rho_1 s_1 & a_2 s_1^2 \end{pmatrix}$$

$$\mathcal{L}_+^1 + \mathcal{L}_-^1 = -2\Delta\omega\,\mathrm{diag}(1,b) + 2q_{0,1}^2(r)\begin{pmatrix} 2a_1\rho_1^2 + s_1^2 & \rho_1 s_1 \\ \rho_1 s_1 & \rho_1^2 + 2a_2 s_1^2 \end{pmatrix}.$$

In using Eq. (4.3) along with the expressions in Eq. (2.23) and Eq. (4.7) it is seen that

$$\boldsymbol{S}_\mathrm{c} = 2g\begin{pmatrix} 0 & a_1\rho_1^2 & \mathrm{i}a_1\rho_1^2 & 0 & \rho_1 s_1 & \mathrm{i}\rho_1 s_1 \\ 0 & \rho_1 s_1 & \mathrm{i}\rho_1 s_1 & 0 & a_2 s_1^2 & \mathrm{i}a_2 s_1^2 \end{pmatrix}, \quad \boldsymbol{S}_- = 2g\begin{pmatrix} 4a_1\rho_1^2 & 4\rho_1 s_1 \\ 4\rho_1 s_1 & 4a_2 s_1^2 \end{pmatrix},$$

and

$$\boldsymbol{S}_+ = 2g\begin{pmatrix} -2s_1^2 & 0 & 0 & 2\rho_1 s_1 & 0 & 0 \\ 0 & 2a_1\rho_1^2 - s_1^2 & 0 & 0 & 3\rho_1 s_1/2 & 0 \\ 0 & 0 & 2a_1\rho_1^2 - s_1^2 & 0 & 0 & 3\rho_1 s_1/2 \\ 2\rho_1 s_1 & 0 & 0 & -2\rho_1^2 & 0 & 0 \\ 0 & 3\rho_1 s_1/2 & 0 & 0 & -\rho_1^2 + 2a_2 s_1^2 & 0 \\ 0 & 0 & 3\rho_1 s_1/2 & 0 & 0 & -\rho_1^2 + 2a_2 s_1^2 \end{pmatrix}.$$

When considering Eq. (4.3) at the limits $b = 1/a_1, a_2$ one has the semisimple eigenvalues

$$b = 1/a_1:\ \mathrm{i}\frac{\lambda_1}{g} = \frac{1}{4a_1}; \quad b = a_2:\ \mathrm{i}\frac{\lambda_1}{g} = \frac{1}{4}.$$

All of the other eigenvalues are simple with zero real part; hence, for small perturbations they will remain purely imaginary. Unlike the previous problems, one must go to higher order in the Taylor expansion in order to capture the leading order behavior of the eigenvalues. Upon doing so one sees that

$$b = 1/a_1:\ \left(\mathrm{i}\frac{\lambda_1}{g} - \frac{1}{4a_1}\right)^2 + c_{b\lambda}^1\left(b - \frac{1}{a_1}\right)\left(\mathrm{i}\frac{\lambda_1}{g} - \frac{1}{4a_1}\right) + c_{bb}^1\left(b - \frac{1}{a_1}\right)^2 = 0, \tag{4.12}$$

and

$$b = a_2:\ \left(\mathrm{i}\frac{\lambda_1}{g} - \frac{1}{4}\right)^2 + c_{b\lambda}^2(b - a_2)\left(\mathrm{i}\frac{\lambda_1}{g} - \frac{1}{4}\right) + c_{bb}^2(b - a_2)^2 = 0, \tag{4.13}$$

where the coefficients $c_{b\lambda}^{1,2}, c_{bb}^{1,2}$ are complicated real-valued algebraic expressions in a_1, a_2. Solving Eq. (4.12) eventually yields that

$$b = 1/a_1:\ 2\left(\mathrm{i}\frac{\lambda_1}{g} - \frac{1}{4}\right) = \left(-c_{b\lambda}^2 \pm \frac{a_1(a_1+2)^2}{8(2a_1+1)(a_1a_2-1)(6a_1^2+2a_1-1)}\right)\left(b - \frac{1}{a_1}\right), \tag{4.14}$$

and solving Eq. (4.13) eventually yields

$$b = a_2 : \; 2\left(\mathrm{i}\frac{\lambda_1}{g} - \frac{1}{4a_1}\right) = \left(-c^1_{b\lambda} \pm \frac{(a_2+2)^2}{8(2a_2+1)(a_1a_2-1)(6a_2^2+2a_2-1)}\right)(b-a_2)\,. \qquad (4.15)$$

An examination of Eq. (4.14) and Eq. (4.15) yields that $\mathrm{Re}\,\lambda_1 = 0$ in for both $a_1a_2 > 1$ and $a_1a_2 < 1$ near the two limits. In conclusion, there is no Hamiltonian-Hopf bifurcation at either limit. Numerical results for the case of the experimental parameters $(a_1, a_2) = (1.03, 0.9717)$ show that there is no bifurcation for all relevant b values.

5. Numerical results

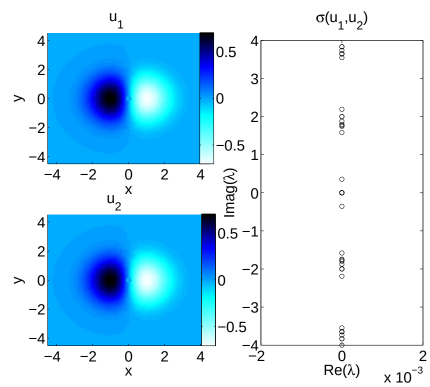

Figure 5: (color online) In-phase dipole, $\mathrm{DD_i}$ ($R = 1$). Colorbars are consistent between this and the following two figures.

The numerical results will be organized as follows. In the first subsection we will confirm the analytical predictions from the previous sections for a physically relevant set of interaction parameters, namely $a_1 = 1.03$ and $a_2 = 0.9717$ for ^{87}Rb [**35**], and monitor the solution branches as a function of R, the ratio between number of atoms in each component. In the next subsection we will explore the dynamical evolution of unstable solutions for some representative regimes of R.

5.1. *Numerical existence and stability*

The numerical results for existence and stability were obtained in a rescaled ($\tilde{r} = r/L$) radial domain $(r, \theta) \in (0, L) \times [0, 2\pi)$ with a Chebyshev basis in r (20 modes) and a Fourier basis in θ (20 modes) as suggested in [**48**, Chap. 11]. For our present computations we set $L = 4.5$. A typical solution pertaining to the stable $\mathrm{DD_i}$ family ($R = 1$) is presented in Figure 5 along with its spectral stability. Since we believe that the most interesting solution branch is attached to the AD solutions, we perform a continuation for the $\mathrm{DD_o}$/AD branches in $R = N_1/N_2$ [1] for fixed $N_1 + N_2 = 5$ and $R \in [0.01, 100]$ (see Figure 6). The continuation begins with a $\mathrm{DD_o}$ solution for $R = 0.01$. Solutions in this regime are stable as in the single component limit, with most of the mass in the second component. The profiles of the two components and the associated linearization spectra for $R = 0.01$, depicted by a magenta circle in Figure 6, are displayed in the left-hand panels of Figure 7. As R is increased there are two Hamiltonian-Hopf bifurcations arising whose eigenvalue trajectories are shown by the real part of the relevant eigenvalue in the first quadrant of the complex spectral plane $\mathrm{Re}(\lambda_{h1})$ in thick dashed blue and $\mathrm{Re}(\lambda_{h2})$ in thick dashed-dotted magenta. The inset,

[1] We define the measure $N_j = \sum_{m,n} |U^j_{m,n}|^2 r_m \Delta r_m \Delta\theta_n$, where $U^j_{m,n}$ is the numerical representation of component j in the radial domain at the grid point (r_m, θ_n) and $\Delta r_m = r_{m+1} - r_m$ (this value is within 1% of that obtained with Clenshaw-Curtis quadrature for the same integral).

and the inset of the inset, depict a zoomed in region just before $R^-_{\mathrm{DD_o}}$ (thin solid red), where a real eigenvalue pair bifurcates from an imaginary one through the origin (thick solid black) for the $\mathrm{DD_o}$ branch, until after R_{AD} (thin dashed-dotted magenta), where, for the newly bifurcating AD branch, the reverse bifurcation occurs and the solution restabilizes. In between, the bifurcation of the AD branch of solutions at $1/a_1$ (thin dashed blue) has materialized, and past the bifurcation point it is this latter branch that is followed (hence the stabilization at R_{AD} vs. $R^+_{\mathrm{DD_o}}$). Notice the very close proximity of these instability and bifurcation phenomena as a function of variations of R, which is induced by the fact that $a_2 - 1/a_1 = 8.26 \times 10^{-4}$ in ^{87}Rb. Unstable solutions before ($R = 0.97$, red circle) and after ($R = 0.9712$, green circle) this bifurcation are shown in the right-hand panels of Figure 7 and Figure 8, respectively. The solution corresponding to $R = 57$ (blue circle) is presented in the left-hand panels of Figure 8. We make note that the predictions for the Hamiltonian-Hopf bifurcations of the real solutions were indeed confirmed, but for $N_1 + N_2 \sim 0.1$ in the limits of small and large R. The inverse bifurcations occur for $N_1 + N_2 < 1$.

5.2. *Dynamics of spectrally unstable states*

In this section we will investigate the dynamics of solutions from the families depicted in Figure 6 with predominantly one component in each of the unstable $\mathrm{DD_o}$ (small R) and AD (large R) regimes, as well as one from the roughly equal atom number regime in which the AD and $\mathrm{DD_o}$ solutions are perturbations of one another. Movies of the dynamics are available online. In order to monitor the detailed instability dynamics, we use a transformed Cartesian domain (with second-order finite-difference Laplacian) for the dynamics, with a fourth order Runge-Kutta integration scheme.[2] The integration is always done for $u(0) = U_s(1+U_r)$ where U_s is the stationary solution in the Cartesian domain and U_r is a random noise field uniformly distributed in the interval $(-0.05, 0.05)$.

There are similarities in the dynamics of the different cases presented, but nonetheless, they are qualitatively distinct. In particular, vortices nucleate as a result of the evolution for all unstable dipole solutions. For the largely asymmetric $\mathrm{DD_o}$ solution depicted in Figure 9 for $R = 0.2642$, the dynamics occur in the direction of the x-axis (over which the larger magnitude component is symmetric) for a long time after the instability initially sets in. The amplitudes appear to remain roughly symmetric over the x-axis, while the vorticity is anti-symmetric. Increasing vorticity seems to emerge in the pattern at larger times. For the comparable atom number case of $R = 0.9712$ (see Figure 10) the dynamics are roughly the same between components, and initially vortices nucleate and annihilate each other in the central density minima of each component as the two lobes breathe smaller and larger (leading to asymmetric density profiles). Again the vorticity increases with time and ultimately, the original structure gets completely destroyed in favor of rotating structures with persistent vortices in both components. When the persistent vortices first emerge around $t = 120$, there is a single dominant one in each component with smaller magnitude ones of inconsistent vorticity magnitude surrounding it in the periphery of the cloud. The largest magnitude vortex in u_1 is negative, while that of u_2 is positive.[3] As expected, these precess in opposite directions (the direction of their respective rotation), and they appear to interact with one another as seen in Figure 11, as well as with other vortices within each component whose magnitude of vorticity increase with time. In particular, one can observe in the included movie, that around $t = 160$, two positively charged vortices begin to attain the same magnitude, at times, as the originally dominant negatively charged one. This can be compared with the time in which the motion of the two vortices become less synchronized in Figure 11. Lastly, for the asymmetric AD solution with $R = 6.296$, and most of the atoms comprising a vortex in the first component, the mild instability takes some time to set in. After $t = 200$, when it has settled in, the vortex in the first component precesses while vortices nucleate and annihilate in the density minimum of the second component (which again develops asymmetric density modulations), much like the previous case for two dipoles. However, as t approaches 400 the dynamics appears to be settling and approaching a rotated (by slightly over 90 degrees clockwise, i.e. opposite the direction of rotation of the precessing vortex) version of the original configuration. For longer integration times, this procedure periodically repeats, leading to a further rotated

[2] In order to compensate for the reduced accuracy of resolving nucleating vortices, we first interpolate to a finer uniform (r, θ) grid, and then map to Cartesian coordinates. Since the mapping results in a reduction of the number of atoms, the dynamics are all done with $N \approx 4.9$.

[3] Counter-clockwise rotation indicates positive vorticity and clockwise rotation indicates negative vorticity.

version of the original configuration, and so on (see Figure 12). While it is beyond the scope of this paper, we feel that understanding this dynamical behavior is extremely interesting.

References

[**1**] F. Abdullaev and R. Kraenkel. Coherent atomic oscillations and resonances between coupled Bose-Einstein condensates with time-dependent trapping potential. *Phys. Rev. A*, 62:023613, 2000.

[**2**] J.R. Abo-Shaeer, C. Raman, J.M. Vogels, and W. Ketterle. Observation of vortex lattices in Bose-Einstein condensates. *Science*, 292(5516):476–479, 2001.

[**3**] B. Anderson, P. Haljan, C. Regal, D. Feder, L. Collins, C. Clark, and E. Cornell. Watching dark solitons decay into vortex rings in a Bose-Einstein condensate. *Phys. Rev. Lett.*, 86(14):2926–2929, 2001.

[**4**] B. Anderson, K. Dholakia, and E. Wright. Atomic-phase interference devices based on ring-shaped Bose-Einstein condensates: two-ring case. *Phys. Rev. A*, 67(3):033601, 2003.

[**5**] P. Ao and S.T. Chui. Binary bose-einstein condensate mixtures in weakly and strongly segregated phases. *Phys. Rev. A*, 58:4836–4840, 1997.

[**6**] R. Battye, N. Cooper, and P. Sutcliffe. Stable Skyrmions in two-component Bose-Einstein condensates. *Phys. Rev. Lett.*, 88(8):080401, 2002.

[**7**] C. Becker, S. Stellmer, P. Soltan-Panahi, S. Dörscher, M. Baumert, E.-M. Richter, J. Kronjäger, K. Bongs, and K. Sengstock. Oscillations and interactions of dark and dark-bright solitons in bose-einstein condensates. *Nature Phys.*, 4:496–501, 2008.

[**8**] R. Bradley, B. Deconinck, and J. Kutz. Exact nonstationary solutions to the mean-field equations of motion for two-component Bose-Einstein condensates in periodic potentials. *J. Phys. A: Math. Gen.*, 38:1901–1916, 2005.

[**9**] S. Burger, K. Bongs, S. Dettmer, W. Ertmer, K. Sengstock, A. Sanpera, G. Shlyapnikov, and M. Lewenstein. Dark solitons in Bose-Einstein condensates. *Phys. Rev. Lett.*, 83:5198–5201, 1999.

[**10**] Th. Busch, J.I. Cirac, V.M. Perez-Garcia, and P. Zoller. Stability and collective excitations of a two-component condensed gas: a moment approach. *Phys. Rev. A*, 56:2978–2983, 1997.

[**11**] P. Chossat and R. Lauterbach. *Methods in Equivariant Bifurcations and Dynamical Systems*, volume 15 of *Advanced Series in Nonlinear Dynamics*. World Scientific, 2000.

[**12**] J. Denschlag, J. Simsarian, D. Feder, C. Clark, L. Collins, J. Cubizolles, L. Deng, E. Hagley, K. Helmerson, W. Reinhardt, S. Rolston, B. Schneider, and W. Phillips. Generating solitons by phase engineering of a Bose-Einstein condensate. *Science*, 287:97–101, 2000.

[**13**] Z. Dutton, M. Budde, C. Slowe, and L.V. Hau. Observation of quantum shock waves created with ultra-compressed slow light pulses in a bose-einstein condensate. *Science*, 293:663–668, 2001.

[**14**] B. Eiermann, T. Anker, M. Albiez, M. Taglieber, P. Trertlein, K.-P. Marzlin, and M. Oberthaler. Bright Bose-Einstein gap solitons of atoms with repulsive interactions. *Phys. Rev. Lett.*, 92(23):230401, 2004.

[**15**] P. Engels, I. Coddington, P.C. Haljan, and E.A. Cornell. Nonequilibrium effects of anisotropic compression applied to vortex lattices in bose-einstein condensates. *Phys. Rev. Lett.*, 89(10):100403, 2002.

[**16**] B.D. Esry and C.H. Greene. Low-lying excitations of double Bose-Einstein condensates. *Phys. Rev. A*, 57: 1265–1271, 1998.

[**17**] B.D. Esry, C.H. Greene, J.P. Burke, and J.L. Bohn. Hartree-Fock theory for double condensates. *Phys. Rev. Lett.*, 78:3594–3597, 1997.

[**18**] E.V. Goldstein and P. Meystre. Quasiparticle instabilities in multicomponent atomic condensates. *Phys. Rev. A*, 55:2935–2940, 1997.

[**19**] R. Graham and D. Walls. Collective excitations of trapped binary mixtures of Bose-Einstein gases. *Phys. Rev. A*, 57:484–487, 1998.

[**20**] D. Hall, M. Matthews, J. Ensher, C. Wieman, and E. Cornell. Dynamics of component separation in a binary mixture of Bose-Einstein condensates. *Phys. Rev. Lett.*, 81:1539–1542, 1998.

[**21**] T.-L. Ho and V. Shenoy. Binary mixtures of Bose condensates of alkali atoms. *Phys. Rev. Lett.*, 77:3276–3279, 1996.

[**22**] M. Hărăguş and T. Kapitula. On the spectra of periodic waves for infinite-dimensional Hamiltonian systems. *Physica D*, 237(20):2649–2671, 2008.

[**23**] T. Kapitula, P. Kevrekidis, and B. Sandstede. Counting eigenvalues via the Krein signature in infinite-dimensional Hamiltonian systems. *Physica D*, 195(3&4):263–282, 2004.

[**24**] T. Kapitula, P. Kevrekidis, and B. Sandstede. Addendum: Counting eigenvalues via the Krein signature in infinite-dimensional Hamiltonian systems. *Physica D*, 201(1&2):199–201, 2005.

[**25**] T. Kapitula, P. Kevrekidis, and Z. Chen. Three is a crowd: Solitary waves in photorefractive media with three potential wells. *SIAM J. Appl. Dyn. Sys.*, 5(4):598–633, 2006.

[**26**] T. Kapitula, P. Kevrekidis, and R. Carretero-González. Rotating matter waves in Bose-Einstein condensates. *Physica D*, 233(2):112–137, 2007.

[**27**] K. Kasamatsu, M. Tsubota, and M. Ueda. Quadrupole and scissors modes and nonlinear mode coupling in trapped two-component Bose-Einstein condensates. *Phys. Rev. A*, 69(4):043621, 2004.

[**28**] P. Kevrekidis, H. Nistazakis, D. Frantzeskakis, B. Malomed, and R. Carretero-González. Families of matter-waves in two-component Bose-Einstein condensates. *Eur. Phys. J. D*, 28:181–185, 2004.

[**29**] P.G. Kevrekidis, D.J. Frantzeskakis, and R. Carretero-González. *Emergent Nonlinear Phenomena in Bose-Einstein Condensates*. Springer-Verlag, 2008.

[**30**] L. Khaykovich, F. Schreck, G. Ferrari, T. Bourdeland J. Cubizolles, L. Carr, Y. Castin, and C. Salomon. Formation of a matter-wave bright soliton. *Science*, 296:1290–1293, 2002.

[**31**] C.K. Law, H. Pu, N.P. Bigelow, and J.H. Eberly. Stability signature in two-species dilute Bose-Einstein condensates. *Phys. Rev. Lett.*, 79:3105–3108, 1997.

[**32**] R. MacKay. Stability of equilibria of Hamiltonian systems. In R. MacKay and J. Meiss, editors, *Hamiltonian Dynamical Systems*, pages 137–153. Adam Hilger, 1987.

[**33**] K.W. Madison, F. Chevy, W. Wohlleben, and J. Dalibard. Vortices formation in a stirred Bose-Einstein condensate. *Phys. Rev. Lett.*, 84:806–809, 2000.

[**34**] M. Matthews, B. Anderson, P. Haljan, D. Hall, C. Wieman, and E. Cornell. Vortices in a Bose-Einstein condensate. *Phys. Rev. Lett.*, 83(13):2498–2501, 1999.

[**35**] K. Mertes, J.W. Merrill, R. Carretero-González, D.J. Frantzeskakis, P.G. Kevrekidis, and D.S. Hall. Nonequilibrium dynamics and superfluid ring excitations in binary Bose-Einstein condensates. *Phys. Rev. Lett.*, 99:190402, 2007.

[**36**] H.-J. Miesner, D.M. Stamper-Kurn, J. Stenger, S. Inouye, A.P. Chikkatur, and W. Ketterle. Observation of metastable states in spinor Bose-Einstein condensates. *Phys. Rev. Lett.*, 82:2228–2231, 1999.

[**37**] C. Myatt, E. Burt, R. Ghrist, E. Cornell, and C. Wieman. Production of two overlapping Bose-Einstein condensates by sympathetic cooling. *Phys. Rev. Lett.*, 78:586–589, 1997.

[**38**] S.B. Papp, J.M. Pino, and C.E. Wieman. Tunable miscibility in a dual-species Bose-Einstein condensate. *Phys. Rev. Lett.*, 101:040402, 2008.

[**39**] D. Pelinovsky and J. Yang. Instabilities of multihump vector solitons in coupled nonlinear Schrödinger equations. *Stud. Appl. Math.*, 115(1):109–137, 2005.

[**40**] V.M. Pérez-García and J. Belmonte-Beitia. Symbiotic solitons in heteronuclear multicomponent Bose-Einstein condensates. *Phys. Rev. A*, 72:033620, 2005.

[**41**] C. Pethick and H. Smith. *Bose-Einstein Condensation in Dilute Gases*. Cambridge University Press, 2002.

[**42**] L. Pitaevskii and S. Stringari. *Bose-Einstein Condensation*. Oxford University Press, Oxford, 2003.

[**43**] H. Pu and N.P. Bigelow. Collective excitations, metastability and nonlinear response of a trapped two-species Bose-Einstein condensate. *Phys. Rev. Lett.*, 80:1134–1137, 1998.

[**44**] V. Schweikhard, I. Coddington, P. Engels, S. Tung, and E. Cornell. Vortex-lattice dynamics in rotating spinor Bose-Einstein condensates. *Phys. Rev. Lett.*, 93(21):210403, 2004.

[**45**] D. Stamper-Kurn, M. Andrews, A. Chikkatur, S. Inouye, H.-J. Miesner, J. Stenger, and W. Ketterle. Optical confinement of a Bose-Einstein condensate. *Phys. Rev. Lett.*, 80:2027–2030, 1998.

[**46**] J. Stenger, S. Inouye, D.M. Stamper-Kurn, H.-J. Miesner, A.P. Chikkatur, and W. Ketterle. Spin domains in ground state spinor Bose-Einstein condensates. *Phys. Rev. Lett.*, 396:345–348, 1998.

[**47**] K. Strecker, G. Partridge, A. Truscott, and R. Hulet. Formation and propagation of matter-wave soliton trains. *Nature*, 417:150–153, 2002.

[**48**] L. Trefethen. *Spectral Methods in MATLAB*. SIAM, 2000.

[**49**] M. Trippenbach, K. Góral, K. Rzazewski, B. Malomed, and Y.B. Band. Structure of binary Bose-Einstein condensates. *J. Phys. B: At. Mol. Opt. Phys.*, 33:4017–4031, 2000.

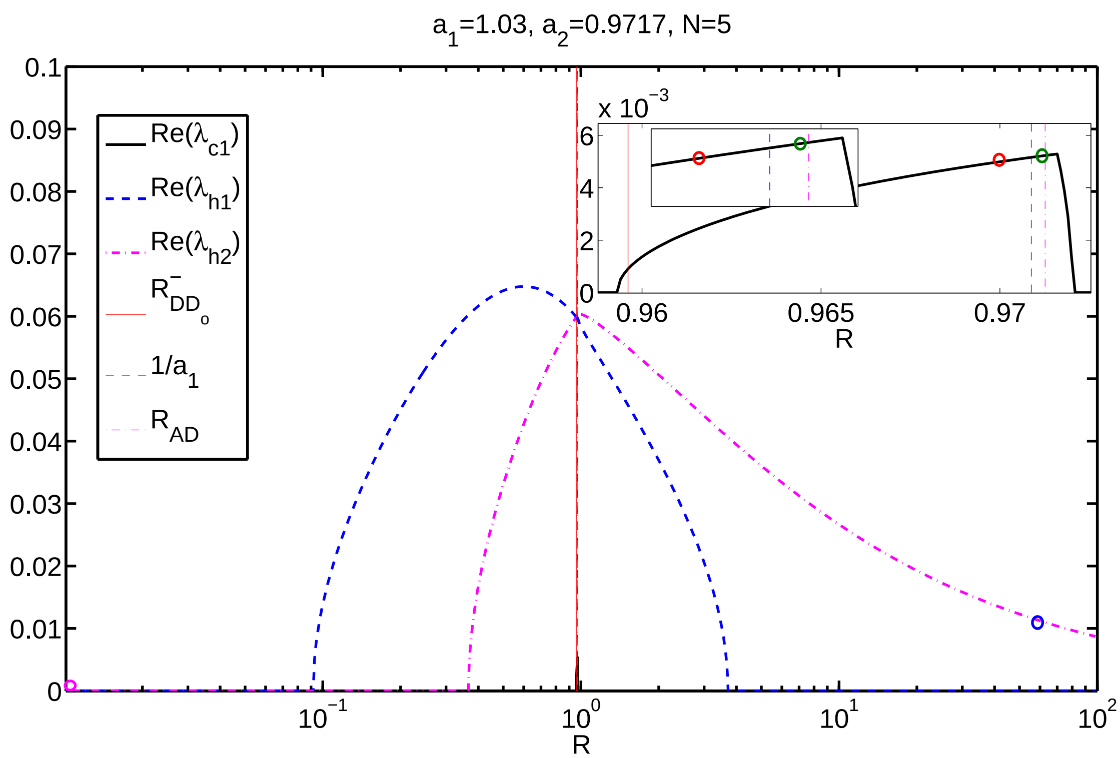

Figure 6: (color online) Diagram of the stability of a branch of solutions which originates from a single dipole as a function of $R = N_1/N_2$, the ratio of the number of atoms of species 1 to that of species 2 ($N = N_1 + N_2 = 5$ remains constant throughout). The far left of the diagram begins from $R = 0.01$, when the first component is very slightly populated out-of phase ($\mathrm{DD_o}$ solution). There are two Hamiltonian-Hopf bifurcations, whose trajectories are indicated by thick dashed (blue) and dashed-dotted (magenta) lines. There is one bifurcation of pure imaginary eigenvalues to pure real through the origin given by the thick solid (black) line at $R^-_{\mathrm{DD_o}}$ (thin solid red line), followed by a structural bifurcation of the solution from DD_o to the azimuthon-dipole solution AD at $1/a_1$ (thin dashed blue), at which point the phase of the first component acquires nontrivial phase, i.e., it becomes a vortex. The real pair of eigenvalues subsequently bifurcates through the origin again just slightly beyond the predicted value R_{AD} (thin dashed-dotted magenta). Notice the inset and the inset of the inset, which zoom in from just before $R^-_{\mathrm{DD_o}}$ to just after R_{AD} (solutions given in Figure 7 and Figure 8 are marked with circles). Then, following the AD branch, we observe an inverse Hamiltonian-Hopf bifurcation, while the second quartet persists until the end of the plot when $R \approx 100$. There will necessarily be another inverse Hamiltonian-Hopf bifurcation when the second component eventually disappears as $R \to \infty$, since the single-charge one-component vortex is linearly stable. However, a continuation until $R > 300$ has been done and $\mathrm{Re}(\lambda_{h2})$ is still non-zero.

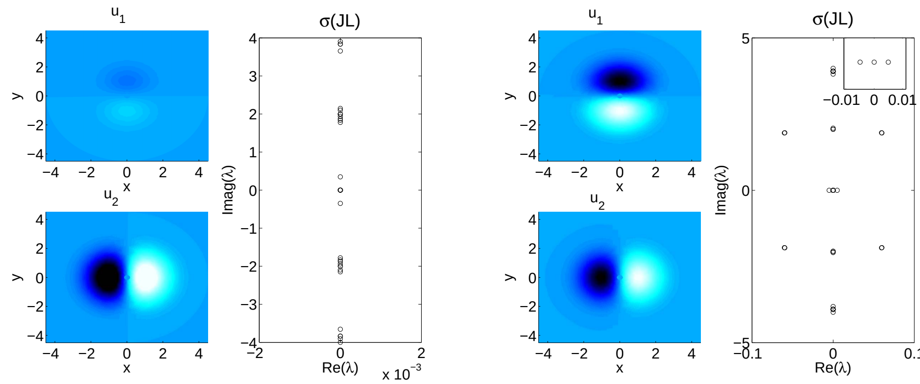

Figure 7: (color online) Out-of-phase dipole, $\mathrm{DD_o}$, is shown for stable ($R = 0.01 < R_-$, left) and unstable ($R_- < R = 0.97 < 1/a_1$) values of R

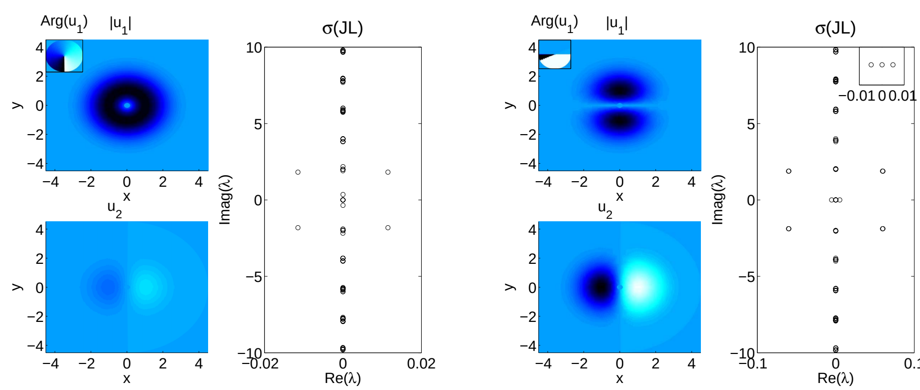

Figure 8: (color online) Azimuthon-dipole, AD, is shown for stable ($R = 57 > R_{\mathrm{AD}}$, left) and unstable ($1/a_1 < R = 0.9712 < R_{\mathrm{AD}}$) values of R.

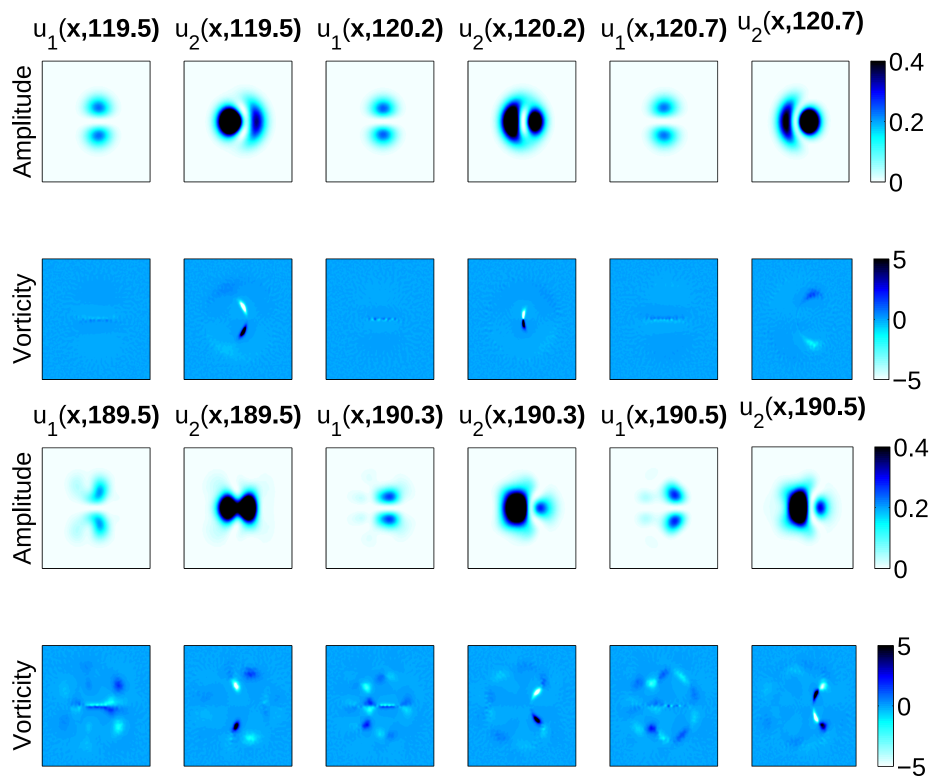

Figure 9: (color online) Some snapshots in the evolution of a solution from the families of Figure 6 for $R = 0.2642$. The amplitude is the squared modulus of the field and the vorticity is the curl of the velocity vector field.

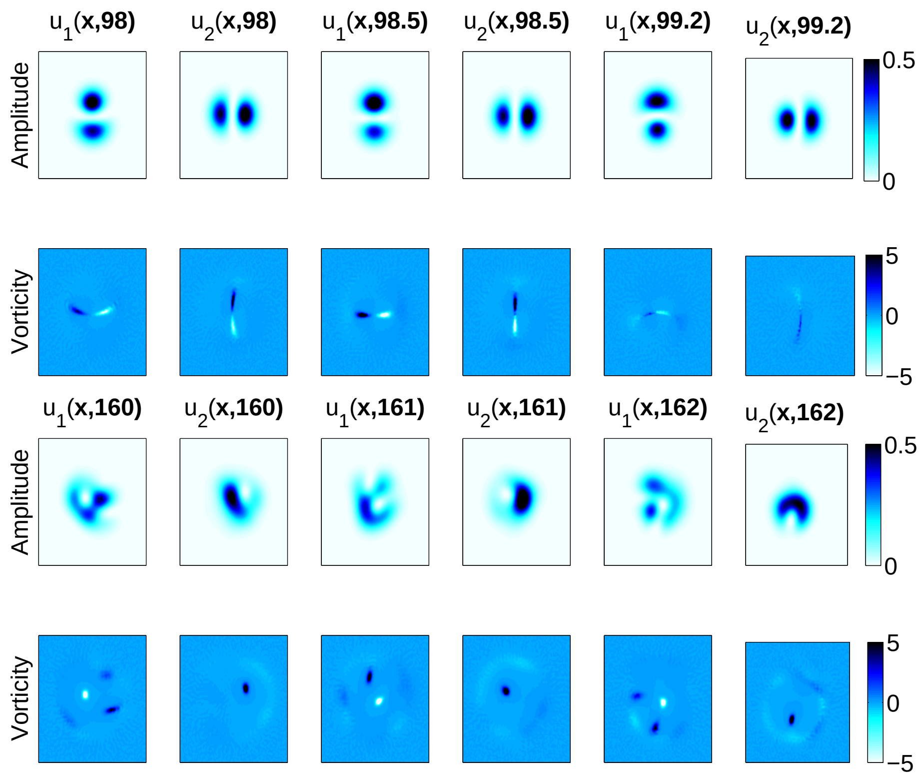

Figure 10: (color online) Some snapshots in the evolution of a solution from the families of Figure 6 for the comparable atom number regime ($R = 0.9712$).

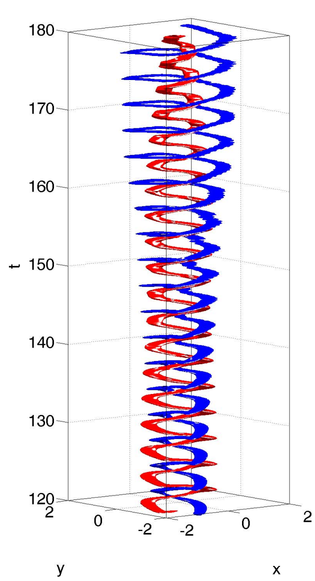

Figure 11: (color online) Vorticity isosurfaces of negative charge in the first component (red) and positive charge in the second component (blue) from the dynamics presented in Fig. Figure 10. The trajectories (clockwise and counter-clockwise, respectively) seem to be synchronized with each other at first and then diverge.

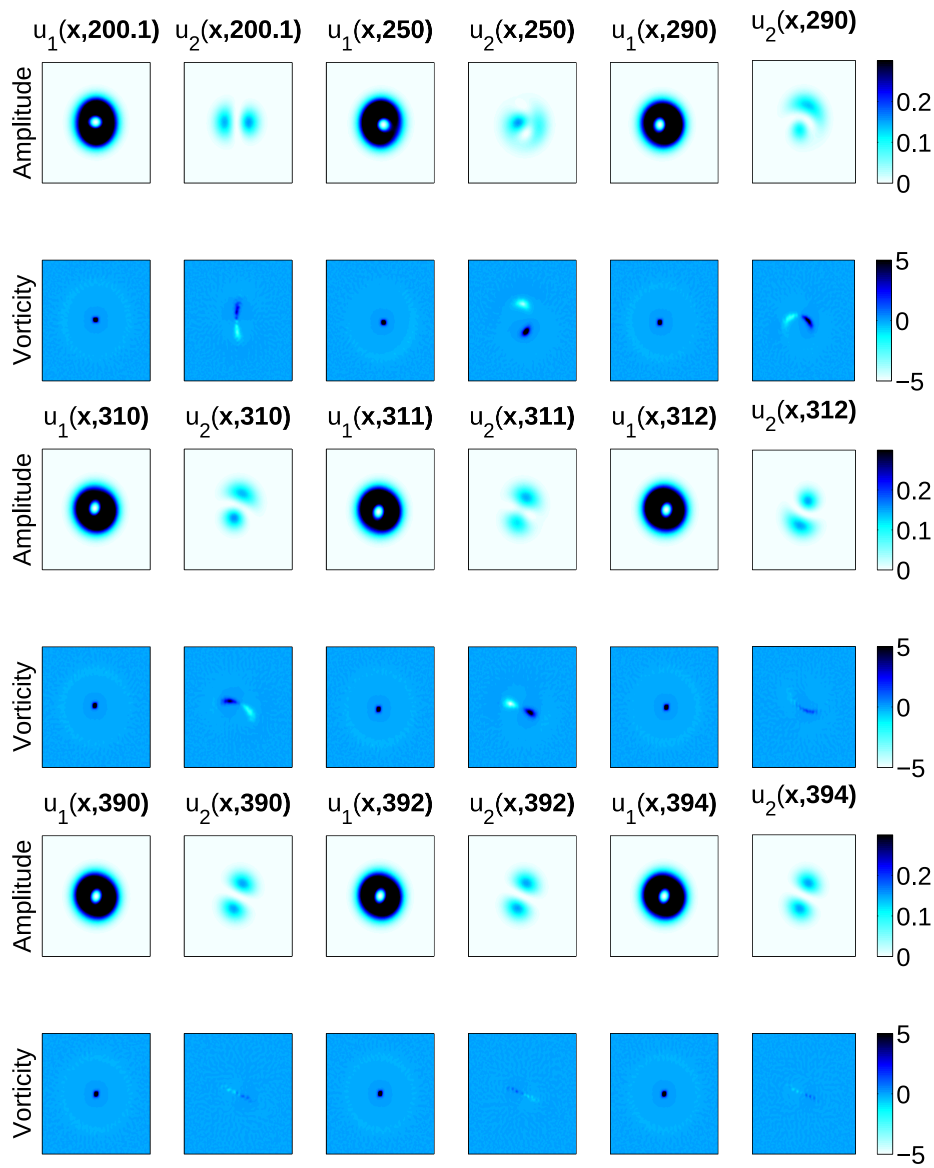

Figure 12: (color online) Some snapshots in the evolution of a solution from the families of Figure 6 for $R \approx 6.296$.